Journal of Materials Science & Technology 168 (2024) 169–184

Contents lists available at ScienceDirect

Journal of Materials Science & Technology

journal homepage: www.elsevier.com/locate/jmst

Review Article

Smart tailoring of molecular catalysts: Mounting approach to oxygen reduction reaction

Anuj Kumar[a,*], Mohd Ubaidullah[b], Guoxin Zhang[c], Jasvinder Kaur[i], Saira Ajmal[d], Mudassir Hasan[h], Krishna Kumar Yadav[f,g], Hafiz M. Adeel Sharif[j,*], Ram K. Gupta[e,*], Ghulam Yasin[d,k,*]

[a] Nano-Technology Research Laboratory, Department of Chemistry, GLA University, Mathura, Uttar Pradesh 281406, India
[b] Department of Chemistry, College of Science, King Saud University, Riyadh 11451, Saudi Arabia
[c] Department of Electrical Engineering and Automation, Shandong University of Science and Technology, Qingdao, Shandong 266590, China
[d] Institute for Advanced Study, Shenzhen University, Shenzhen, Guangdong 518060, China
[e] Department of Chemistry, Kansas Polymer Research Center, Pittsburg State University, Pittsburg, KS 66762, United States
[f] Faculty of Science and Technology, Madhyanchal Professional University, Ratibad, Bhopal 462044, India
[g] Environmental and Atmospheric Sciences Research Group, Scientific Research Center, Al-Ayen University, Thi-Qar, Nasiriyah 64001, Iraq
[h] Department of Chemical Engineering King Khalid University, Saudi Arabia
[i] Department of Chemistry, School of Sciences, IFTM University, Moradabad, Uttar Pradesh 244102, India
[j] Research Center for Eco-Environmental Engineering, Dongguan University of Technology, Dongguan 523808, China
[k] School of Environment and Civil Engineering, Dongguan University of Technology, Dongguan, Guangdong 523808, China

ARTICLE INFO

Article history:
Received 24 March 2023
Revised 23 April 2023
Accepted 27 April 2023
Available online 19 June 2023

Keywords:
Electrocatalysis
Molecular catalysts
Oxygen reduction reaction
Sabatier principle

ABSTRACT

Efficient electrocatalytic rupture of energy-rich molecules (H_2 and O_2) is a green approach for generating clean energy for modern societies. In this context, porphyry-type molecular electrocatalysts act intelligently toward oxygen reduction reaction (ORR), a fundamental process in fuel cells, due to their redox-rich chemistry, which involves core metal ions and macrocyclic ligands. The concerned scientific community has tried many times to correlate the ORR intermediates with their formation kinetics and simplify the associated multi H^+/e^- stages during the ORR process, constructing several volcano plots between catalytic Tafel data, turnover frequencies, and overpotentials for many electrocatalysts. Despite the fact that many review articles on molecular electrocatalysts for ORR have been published, understanding the strategic implications and molecular catalyst intelligence towards homogenous ORR has been poorly explored. This review examined the relationships between volcano plots of current vs. thermodynamic parameters and the Sabatier principle in order to explain the intelligence of molecular electrocatalysts and approaches for their creation, as well as the difficulties and potential prospects of molecular electrocatalysts. These facts distinguish this review from previously published articles and will pique the scientific community's interest in avoiding trial-and-error procedures for catalyst creation while also allowing for more exact evaluations of the molecular catalyst's performance.

1. Introduction

1.1. Motivation to study oxygen reduction reaction

Rapid depletion of existing conventional fuels to meet global energy needs is not only increasing their prices but also contributing to climate change and inviting serious environmental problems [1,2]. Therefore, it is necessary to find alternative, green, and sustainable energy resources. Within this agenda, the conversion of chemical energy, which is stored in chemical bonds in molecules like H_2, and O_2, into electrical energy via electrochemical strategies can be considered an efficient way to produce clean energy. For

* Corresponding authors.
E-mail addresses: anuj.kumar@gla.ac.in (A. Kumar), hmadeelcmc@hotmail.com (H.M.A. Sharif), ramguptamsu@gmail.com (R.K. Gupta), yasin.bzu@hotmail.com, yasin@mail.buct.edu.cn (G. Yasin).

https://doi.org/10.1016/j.jmst.2023.04.073
1005-0302/

instance, in fuel cells, H_2 and O_2 combine to form water and electricity, involving an extremely slow cathode process, oxygen reduction reaction (ORR), requiring highly robust electrocatalysts [3,4].

1.2. Electrocatalysts for oxygen reduction reaction

From the above-mentioned perspective, Pt-based materials have been deemed promising models to catalyze the ORR process; nevertheless, their scarcity, high price, restricted activity, and durability have hampered their practical applications. These challenges confronting scholars motivate the creation of inexpensive, superior, and durable electrocatalysts for the advancement of the energy sector [5]. Within this agenda, molecular and composite-based electrocatalysts are on trend. Composite-based electrocatalysts have so far shown good activity and stability, with the constraints of easy and precise modifications to further improve their electrocatalytic performances [3,6,7]. Moreover, the precise determination of real active sites and the development of structural-reactivity functional relationships for the composite electrocatalysts are still challenging tasks. These limitations are assumed due to the lack of discrete energy levels in composite-based catalysts. Thus, despite their substantial efforts, scientists remain far from overcoming their constraints and making subsequent progress in avoiding hit-and-trial procedures for their construction [8,9].

In 1971, Jalanshki [10] tested Fe-phthalocyanine (a synthetic analogue of Fe-porphyrin with FeN_4-moieties as the active site for O_2 binding) for oxygen reduction reactions electrochemically for the first time. After that, the concerned scientific community tested similar metal-N_4-molecular systems, including porphyrin [11] and phthalocyanine and their analogues, with a variety of transition metals for the same purpose. But Fe-N_4 molecules (Fe-phthalocyanines, in particular [12]), since they possess the optimal electronic and geometrical features, can reduce O_2 efficiently, and therefore Fe-molecular systems can be considered ideal models for ORR.

In particular, Fe-porphyry type molecular systems can be easily modified via chemical treatment to improve their reactivity and selectivity towards ORR, making them far superior to composite-based electrocatalysts [13–15]. More importantly, for molecular electrocatalysts, the turnover frequency (TOF), as well as overpotential, can be related by creating their catalytic Tafel plots [16]. This approach examines the intrinsic properties of molecular electrocatalysts, offering their benchmark electrocatalytic ORR performance [17]. In addition, molecular systems have discrete energy levels that can be altered by modifying their macrocyclic core to optimize their electronic as well as electrocatalytic properties [18,19]. Therefore, substitution effects on their catalytic Tafel plots make it possible to act intelligently towards ORR. Fig. 1 shows the systematic illustration of the intelligence of Fe-based molecular catalysts during ORR via several factors, including pull-push, inductive, axial, co-facial, and second coordination sphere effects. Molecular electrocatalysts act as redox mediators during ORR, therefore, the above-mentioned intelligence effects can alter the redox potential of these catalysts, benefiting their ORR activity [20]. Besides, several factors, including substituent effects within the metal's coordination sphere and linear free-energy relationships that arise due to the electronic structure effects, decrease the driving force for the homogeneous ORR by decreasing the maximum rate of reaction [21]. Utilization of these effects in a strategic manner possesses the promise of boosting the catalytic ORR performance of a poor molecular catalyst [22–24].

Although there are many review articles that are reported on molecular electrocatalysts for ORR, the understanding of these strategic effects and molecular catalyst's intelligence towards homogenous ORR is poorly discussed in the literature, which motivated us to organize this review article. Herein, we discuss the thermodynamics of ORR for the fundamental understanding of the ORR mechanism with homogenous molecular electrocatalysts. Further, we emphasized the intelligence of molecular electrocatalysts, highlighting the electronic as well as electrochemical features and their correlations with electrocatalytic ORR activity by means of volcano plots under the light of Sabatier's principle [23,25]. We believe that this mini-review article will build on the fundamental concepts of science and engineering to design smart electrocatalysts and to enjoy their intelligence not only for ORR but also for other electrocatalytic reactions. The beginners will get a critical understanding of ORR mechanisms and other parameters, including overpotential, TOF, catalytic Tafel plots, etc. Because molecular electrocatalysts (MN_4 molecular systems) [26] and atomically dispersed single-atom/dual-atom metal-nitrogen-carbon (M-N-C) materials possess similarities, this review article will also help researchers to understand the role of active sites during electrocatalysis and how their catalytic performance can be improved further by using the strategies discussed in this review.

2. Fundamental of ORR process with molecular electrocatalysts

Molecular catalysts are catalysts with controllable size, composition, and reactivity, making them preferable to other types of catalysts with the advantage of comparative investigation isolating the influence of structural and electrical modifications to the catalyst. Many of them are metal complexes with the ability to be chemically modified to increase the rate of chemical reactions [27]. On the other hand, when these molecular catalysts allow an extra electron transfer step with the electrode in the electrolyte to be dispersed thoroughly into the reaction system, they become homogenous molecular catalysts and can offer active sites for ORR, this process is termed homogenous ORR [28,29].

Since the reaction rates of the molecular electrocatalysts of relevance for practical applications are so high, the steps in their cycle that dictate the reaction rate occur inside the diffusion layer close to the electrode. Most of the homogeneous molecular catalysts never participate in the reaction at all. A stock of them, however, might be utilized to maintain a constant catalyst concentration in the diffusion-reaction layer [30]. Since electrode potential can change, the abscissa of the catalytic Tafel plots for overpotential can shift as well [31]. This phenomenon does not imply that the driving force for the homogeneous reaction changes, but rather that the concentration of the catalyst at the electrode changes. The Nernst equation is met by the rapid electron transport provided by the homogeneous molecular catalyst. In the following subsections, we briefly reviewed the approaches that can be used to evaluate ORR's efficacy, as well as the concepts behind using bond dissociation-free energies to evaluate the ORR performance of molecular electrocatalysts [32]. These approaches allow for a direct comparison of the performance of different homogeneous electrocatalysts in a wide diversity of experimental conditions.

2.1. ORR efficiency and overpotential

In order to better understand and develop superior molecular electrocatalysts, it is essential to determine the overall ORR efficiency of such molecular electrocatalysts. Molecular electrocatalysts should be able to maintain high catalytic rates for a long time. Keeping these criteria in mind, electronic properties that are used to measure the ORR efficiency, such as turnover number, TOF, and overpotential (η), are necessary to explore, as discussed in Section 3. In addition to this, the optimal ORR catalysts exhibit particular product formations like water vs peroxide [33]. Therefore, it is common practice to investigate ORR catalysts over a wide range of experimental conditions, which may include the use of a variety

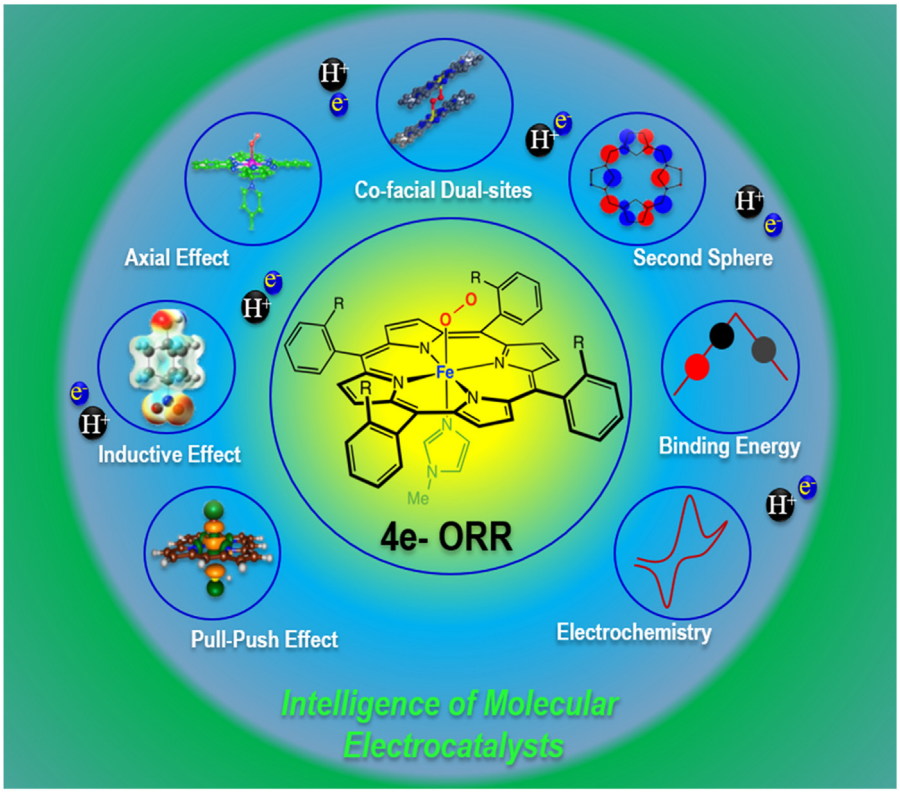

Fig. 1. Illustration of intelligence of molecular electrocatalysts towards ORR.

of solvents and proton sources [21]. Usually, TOF is measured as a ratio between the maximum number of active catalyst molecules and the number of product molecules that are generated in a given amount of time. The value of η can be calculated from the difference between the potential of the electrode and the standard potential of half reaction (denoted by E and $E°_{rxn}$, respectively), and these features are not reliant on the experimental conditions [34].

2.2. Thermochemical cycle for ORR mechanisms

Usually, ORR takes place at the cathode and the intrinsic mechanistic, as well as reaction kinetics, can be investigated using cyclic voltammetry (CV) and linear sweep voltammetry (LSV). These techniques provide the plateau current values as well as half-wave potential ($E_{1/2}$), which allows the establishment of the reaction mechanism and calculation of rate constants. Within this agenda, ORR molecular catalysts should function at potentials near to thermodynamic potential (1.23 V) while retaining speedy ORR kinetics and excellent selectivity (H_2O vs. H_2O_2). The ORR's thermodynamic potential is influenced by two primary reactions: $O_2 + 2H^+ + 2e^- \rightarrow H_2O_2$ and $O_2 + 4H^+ + 4e^- \rightarrow 2H_2O$. Although molecular catalysts can often catalyze both reactions, it is critical to have a solid understanding of the formed products to properly assess and contrast ORR catalysts. Therefore, knowing the pertinent thermochemistry of both the above-mentioned reactions would aid when evaluating ORR catalysts in various media. ORR involves several O-intermediates and multistep of nH^+/e^- transfer. All of the anticipated free intermediates have known reduction potentials and pKa values in H_2O, as shown in Fig. 2(a) (the plot between relative free energy ($nE°$) for O-intermediates and the number of transferred electrons during O_2 reduction at pH = 7) [35].

Many molecular catalysts have been immobilized on carbon surfaces as heterogeneous catalysts and then studied for ORR in aqueous environments; this is necessary because molecular catalysts are insoluble in water and dissolvable in organic solvents like C_3H_7NO (DMF) or CH_3CN (MeCN). One constraint of such investigations was, until recently, a lack of knowledge of the standard or $E_{1/2}$ potential for ORR in such environments. For the first time, the O_2/H_2O standard potentials ($E°_{O2/H2O}$) in CH_3CN and C_3H_7NO were computed in 2015 by Pegis et al. [36] using the thermochemical cycle as depicted in Eqs. (1–5). The direct measurement of the H^+/H_2 couple with a Pt wire is facilitated by the simplicity of this thermochemical cycle, which relies only on the known ORR and H^+/H_2 potentials vs SHE in water, the standard H^+/H_2 potential in nonaqueous environments, and a considerably lower value of $\Delta G°_{H2O}$ (aq→org). It was found that the values of $\Delta G°_{H2O}$ (aq→org) in CH_3CN and C_3H_7NO were -19 and -64 meV, respectively [37]. As a result, the ORR equilibrium potential in a wide range of acidic/organic environments can be approximated as 1.23 V, which is greater than the reported H^+/H_2 potential in similar experimental conditions, assuming that $\Delta G°_{H2O}$ (aq→org) is zero [37].

$$O_{2(g)} + 4H^+_{(eq.)} + 4e^-_{(SHE)} \leftrightarrow 2H_2O_{(aq.)} \; E^o_{O_2/H_2O} \quad (1)$$

$$O_{2(g)} \leftrightarrow 4H^+_{(eq.)} + 4e^-_{(SHE)} \; E^o_{H^+_{aq.}/H_2} \quad (2)$$

$$4H^+_{(org.)} + 4e^-_{(Fc^{+/0})} \leftrightarrow 2H_{2(g)} \; E^o_{H^+_{org.}/H_2} \quad (3)$$

$$2H_2O_{(aq.)} \leftrightarrow 2H_2O_{(org.)} \; \Delta E^o_{H_2O \; (aq.\rightarrow org.)} \quad (4)$$

$$O_{2(g)} + 4H_{(org.)} + 4e^-_{(Fc^{+/0})} \leftrightarrow 2H_2O_{(aq.)} \; E^o_{O_2/H_2O(org.)} \quad (5)$$

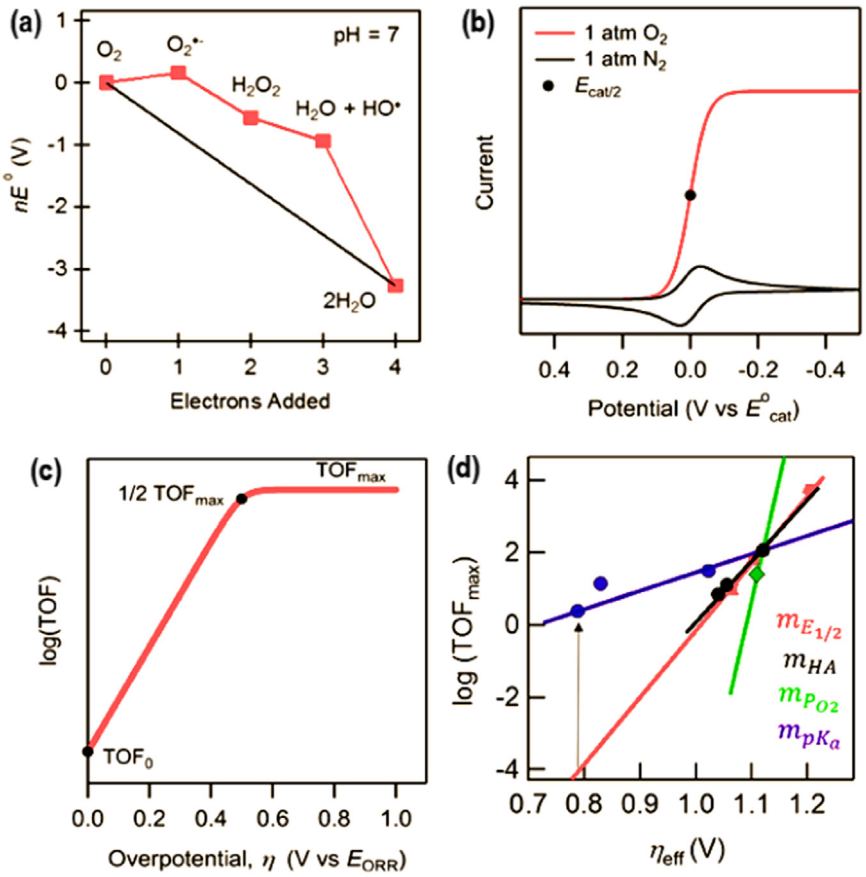

Fig. 2. (a) ORR intermediates potential and electron transfer curve during ORR at pH 7. (b) CVs of a molecular catalyst in the presence and absence of N_2/O_2, with a notation of $E_{cat/2}$. (c) ORR Tafel plots, indicating 1/2 TOF_{max}, TOF, and $E_{cat/2}$ data points. Adapted with permission [35]. Copyright 2014 The Royal Society of Chemistry publishing group. (d) Relationship between log(TOF_{max}) and effective overpotential for Fe-tetraphenyl-porphyrin. Adapted with permission [44], Copyright 2017 American chemical society publishing group.

2.3. Thermodynamics

Overpotential ($\eta = E_{ORR}$ - E_{appl}, where E_{appl} and E_{ORR} are the applied potential and equilibrium potential, respectively) is directly related to thermodynamic parameters, which are required to estimate the overall ORR energy efficiency for homogeneous molecular electrocatalysts. The TOF of the conventional heterogeneous electrocatalyst increases as the overpotential increases. The ORR Efficiency measures in heterogeneous systems are commonly TOF/current density at a constant overpotential [38]. The best electrocatalyst will have the highest TOF at the lowest overpotential at a known current density. In contrast, homogeneous molecular electrocatalysts exhibit a distinctive behavior, since their ideal CVs would possess duck-shaped curves that approach a limiting current at negative potentials.

Fig. 2 shows that the current is restricted by chemical processes in solution even at zero potential, indicating that nearly all of the soluble catalyst has been depleted at this point. A maximum TOF, or TOF_{max}, is reached by the catalyst at these potentials. Typically, catalyst TOF responds to the electrode potential, which is directly related to overpotential, in a Nernstian fashion in the potential-dependent area before the plateaued current. Considering a first-order catalytic mechanism, the log(TOF) vs (Fig. 2(b)) molecular Tafel plots, developed by Artero and Saveant [35], provide a clear relationship between log(TOF) and overpotential (Eq. (6)).

$$TOF = \frac{TOF_{max}}{1 + \exp[\frac{F}{RT}\left(E_{ORR} - E_{\frac{cat}{2}}\right)\exp\left[-\frac{F}{RT}\eta\right]} \quad (6)$$

In a low-overpotential window, the molecular Tafel plot's slope was found to be 59 mV/dec. At the negligible driving force, TOF can be measured by extrapolating the Tafel plot for the heterogeneous electrocatalysts, much like the exchange current density may be computed in a similar way using homogeneous molecular electrocatalysts. The exponential terms in the denominator of Eq. 6 tend toward zero in the higher overpotential window. Almost all of the catalysts have been consumed at this point, displaying an equality of TOF with the TOF_{max} [35]. Therefore, analyzing the log(TOF) at the effective overpotential (Eq. 7) for ORR catalysis is an alternate approach for evaluating catalyst performance [39–41]. The effectivity parameter $\eta_{eff} = E_{ORR}$ - $E_{cat/2}$, where $E_{cat/2}$ is the potential at which the TOF is 1/2 of the maximum TOF ($TOF_{max/2}$) (black dot in Fig. 2(c)). If $E_{cat/2}$ is found to be very close, $E_{cat/2}$ can be replaced by $E_{1/2}$ in the following equation, allowing the direct comparison between effective overpotential and TOF for the different electrocatalysts. This is true, however, only under a narrow range of reaction circumstances, and only when the mechanisms being compared have the same reaction order with the catalyst [28].

$$\eta_{eff} = E_{ORR} - E_{cat/2} \quad (7)$$

In molecular electrocatalysts, one of the most difficult challenges involves precisely quantifying the maximum turnover frequency based on the current which is recorded by cyclic voltammogram. This condition is especially difficult for the four-electron oxidation-reduction reaction. Based upon the homogenous catalysts, the turnover frequency is the moles of product per mole catalysts per unit of time. For molecular imputes, the correlation between the turnover frequency and catalytic current is highly com-

plicated since the reaction takes place only thin solution layer near the electrode surface known as the diffusion layer [42,43]. For the calculation of turnover frequency, the catalysts which occupy the diffusion layer should only be counted.

Within this paradigm, utilizing a Fe-tetraphenylporphyrin molecular electrocatalyst, Pegis et al. [44] demonstrated that scaling relationships of ORR intermediates could be broken. They showed that the TOF_{max} scales with effective overpotential under different reaction circumstances by decoupling the e^-/H^+ transfer pathway for the ORR. Further, it was demonstrated that the scaling of $\log(TOF_{max})$ with effective overpotential can be predicted using the concepts of rate law as well as Nernst law over a wide range of overpotential windows in organic solvents. For instance, changing the O_2 partial pressure (mPO_2), the acid concentration in solution (mHA), the pK_a of the H^+ resource (mpK_a), and the TOF_{max} with the Fe^{3+}/Fe^{2+} redox potential ($mE_{1/2}$) yields multiple slopes ($\log(TOF_{max})$/eff) (Fig. 2(d)) [35,39]. The arrow in Fig. 2(d) indicates that the ORR driven by organic solvents containing $HOC_6H_4CO_2H$ is 10^4 times faster than predicted by the previous scaling formula based on the catalyst's $E_{1/2}$ [34].

This type of study predicts the existence of such correlations for all molecular electrocatalysts and shows that the kinetics and thermodynamics of catalytic reactions are extremely malleable. Measuring the effective or ordinary overpotential of soluble ORR catalysts under varying conditions makes it possible to compare and benchmark these systems. Electrochemical strategies and soluble reductants are both useful for determining the TOF_{max} of a catalytic system. One can get insight into the current-limiting mechanism and better optimize the catalytic system by studying the dependence of the TOF_{max} and effective overpotential on circumstances (catalyst, proton source, solvent, etc.) [41,45]. Mechanistic insights may inspire readers to change catalyst conditions to reduce effective over potential without reducing maximum turnover frequency. Researchers plan to use soluble catalysts and molecular chemistry to establish structure or activity conditions and improve ORR intermediate energies and batteries. These studies should help to design molecular catalysts and heterogeneous materials for device structure.

Sabatier's principle and volcano plots, which serve as guiding principles to inspire the development of better catalysts, have found widespread use in the study of electrocatalysis mediated by surface active sites, particularly for the electrocatalytic ORR process at the metallic surfaces. Generally, reaction intermediate stabilization not only reduces the activation energy required for formation but also slows the reaction's progression to the final products and the subsequent regeneration of active sites for further catalytic processes. Thus, to maximize the typical rate constant, it is necessary to strike a balance between the above-mentioned outcomes during the catalytic process [46]. In this paradigm, Sabatier's principle demonstrates that a plot of TOF vs. intermediate energy will produce maximum TOF, the volcano's peak, at an energy that corresponds to an intermediate that is neither too static nor too dynamic. Although these ideas were proposed in the late 1950s, they are still the subject of ongoing dispute [47–49], and their use in molecular catalysis has not been as prevalent as in heterogeneous catalysis [39,50].

By displaying TOF vs. primary intermediate stability, it has demonstrated [51] that volcano peaks can arise or go. Their conclusion is conditional on the reaction mechanism and maybe on other variables that change from one electrocatalyst to another one. There is a trade-off between the kinetics of the irreversible homogeneous catalysis that forms C and re-produces catalyst P and the equilibrated formation of reduced catalyst state Q, which leads to the TOF. At a given overpotential, there may be a trade-off between a powerful driving force for the homogeneous catalysis involving Q and the first creation of appropriate Q (Fig. 3(a, b)). This could be the case if the initial creation of adequate Q requires a sufficient amount of Q. Even while the traditional reduction potential is very low for highly negative potentials, the concentrations of Q may greatly increase, which suggests that such a compromise and the subsequent appearance of a volcanic peak may not take place at these extremely negative potentials (Fig. 3(c-e)) [52].

3. Smart tailoring of molecular catalysts towards ORR

Among the most interesting features of molecular catalysts is that they possess distinct frontier energy levels, which can be manipulated via smart tailoring of their molecular core. These tailoring strategies for porphyry-type molecular models include the introduction of electron-donating and -withdrawing groups on the ligand framework, axial ligation, a change in the substituent's position, as well as a change in the secondary coordination sphere, and can offer fine tuning of their frontier energy levels. These frontier energy levels are directly associated with their O_2 binding ability as well as their redox potential, which play a key role during the O_2 catalysis. The entire ORR pathway, including O_2 adsorption as well as its reduction steps on these molecular catalysts, can be controlled by monitoring the energy gap between the highest occupied molecular orbital (HOMO, eg-orbital) of the molecular catalyst and π^* orbital of O_2. The smaller gap between these energy levels can offer the optimum electronic coupling, and the O_2 molecule can be bound tightly on the active site of these molecular catalysts [53–55], improving the O_2 binding energy (E_bO_2). Besides, it is believed that the eg-orbital of the central metal atom of molecular catalysts is associated with their M(III)/M(II) redox potential, which acts as an ORR mediator during ORR. Therefore, tailoring the energy levels of molecular catalysts alters their M(III)/M(II) redox potential [56,57], affecting their ORR activity. In the next sub-sections, a series of influences and smart tailoring strategies to change the detailed catalytic electrochemical performance of molecular electrocatalysts have been discussed in detail.

3.1. Through electron withdrawing/donating substituents

An intriguing property of molecular catalysts is that their electronic structure can be tuned by adjusting their molecular core. In addition, substitution on their molecular core also affects their ORR overpotential as well as the turnover frequency. For instance, electron-withdrawing groups (EWGs) can reduce the electron density on the active site (central metal atom), making the active site more accessible for extra electron injection, allowing the active state of the catalytic site to be accessed at lower potentials and thereby lowering the overpotential [58–60]. Similarly, electron-donating groups (EDGs) on the core of molecular catalysts increase electron density on the active site, making its reduction more difficult and increasing the overpotential towards ORR.

The nature and features of the pre-equilibrium, as well as the rate-determining step (RDS), are also affected by the substituents on the molecular catalyst's core, which in turn impacts their TOF. Whether a pre-equilibrium or RDS [50], the first and most important step in ORR is the binding of O_2 with the active site, producing the O_2-adduct. Therefore, in the context of an electronic push-pull process, the action that makes the overpotential more (or less) favorable is predicted to decrease (or raise) the affinity between the active site and O_2. This justification is based on the 'iron law', which states that modifying a catalyst's substituents changes the catalyst's electronic structure, resulting in a positive change in one parameter but a negative change in another. By analyzing how altering catalyst substituents affect succeeding stages in the reaction mechanism, the reality and degree of this 'iron law' may be proven. For example, tetra-substituted iron porphyrins (Fig. 4(a–g)) displayed $4e^-$ ORR in protonated N, N-dimethylformamide. The

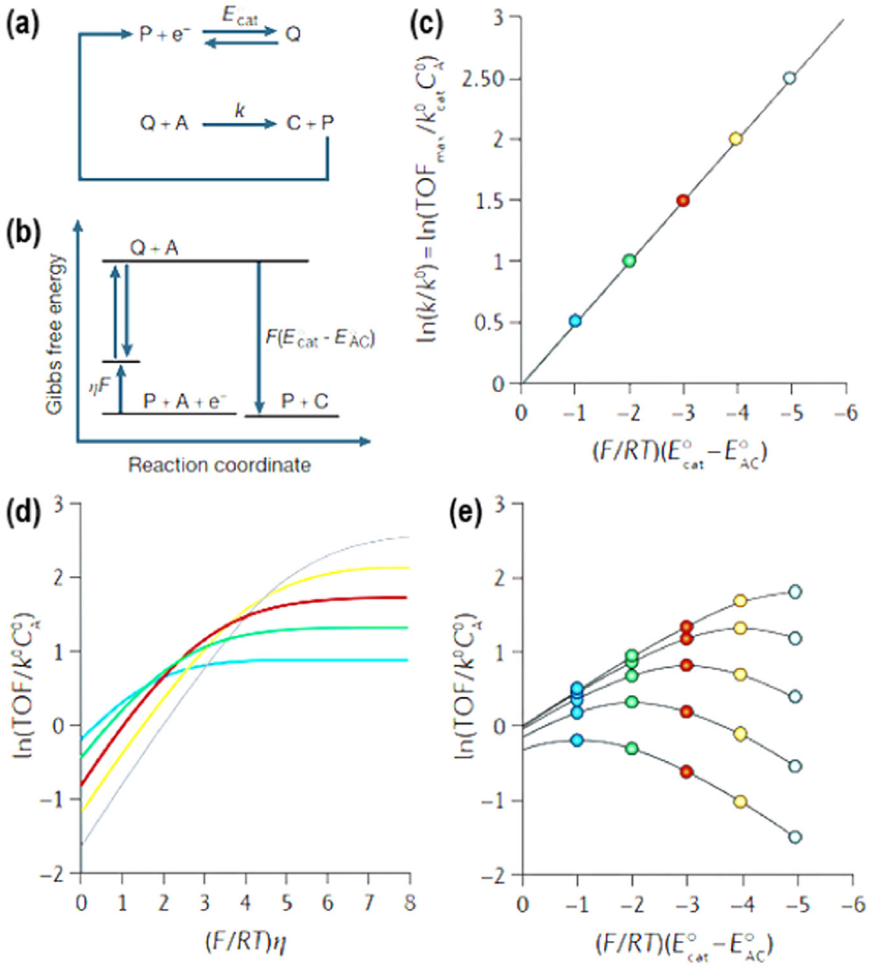

Fig. 3. Scheme for the (a) conversion of reactant into product electrochemically and corresponding rate constants, and (b) free energy curve. (c) The plot between the normalized rate constant, k/k^0, vs. applied driving force for various molecular catalysts. (d) Tafel plots at the potentials mentioned in curve (c), and corresponding (e) Volcano plots simulated. Adapted with permission [51,52], Copyrights 2019 American chemical society publishing group.

most important feature of these molecular models is that they exhibit Fe^{3+}/Fe^{2+} redox couple, which acts as ORR mediator.

Moreover, for these molecular electrocatalysts, the rate of the overall ORR process was found to be dependent on the concentration of both the O_2 and $DMFH^+$, involving the k_1 and k_2 rate constants, as depicted in Fig. 5(a). When E°_{cat} is used as a thermodynamic index, the overall rate constant, $k_{cat} = K_2k_3$, seems to have a strong Hammett-type association with it (Fig. 5(b)). For instance, EDGs with these molecular catalysts increase the basicity of the O_2-adduct and decrease its acidity, making the O_2-adduct protonated more quickly, and vice versa for the catalysts with EWGs. Again, the relationship between TOF and E°_{cat} is steady with the 'iron rule' (Fig. 5(c)), as evidenced by the catalytic Tafel plots in Fig. 3(d).

Recently, Han et al. [61] exhibited significant catalytic activity of FePc in a chemically regenerative redox fuel cell (Fig. 5(d)), which was accomplished by the Fe^{3+}/Fe^{2+} redox pair of FePc. Following the reduction of the Fe^{3+} state of Fe in FePc to a Fe^{2+} state at the carbon electrode surface in the electrolyte, the re-oxidation of the Fe^{2+} state into the Fe^{3+} state of Fe in FePc was begun by O_2 adsorption, resulting in the endowment of $4e^-$ ORR. They hypothesized that first of all, O_2 adsorbs on the Fe^{2+} site of FePc, then O_2 gets reduced, generating an O_2-adduct, which on protonation produces Pc-Fe^{3+} and Pc-Fe^{3+}-O_2H species. The further reduction of H_2O_2 and succeeding intermediates eventually took place on Pc-Fe^{2+}, resulting in H_2O and a free Pc-Fe^{2+} active site, demonstrating an increase in maximum power density from 170 to 249 mW/cm^2 in the process. This improvement shows that using naturally occurring molecular electrocatalysts could be a good way to improve the performance of chemically regenerative redox fuel cells in the future.

3.2. Through axial ligand and substituent's position effects

Most naturally occurring porphyry-type molecular models and their synthetic analogues possess D_{4h} symmetry with a planar tetra-aza environment around the central metal atom. Therefore, axial ligation at the active site is an often-overlooked factor in O_2 binding to molecular catalysts and their subsequent reactivity. Usually, the effect of axial ligation has been the subject of a significant amount of research in the context of heme enzyme reactivity [62–66]. The ORR activity of molecular catalysts is influenced by the electron density on the active site, which is directly affected by axial ligand coordination at the fifth position of the active site. On the other hand, very few studies have investigated how axial ligation affects the overpotential and TOF for ORR using molecular electrocatalysts.

Solomon et al. [67] investigated the effect of axial ligation with a tetrakis(4-N-methylpyridyl)-Fe(III)P (TMPyFe^{3+}P) molecular catalyst on the reduction rate of O_2•. The results revealed that the higher lability of the aqua ligand facilitated the inner-sphere e-transfer path with the direct creation of an O_2-adduct with the

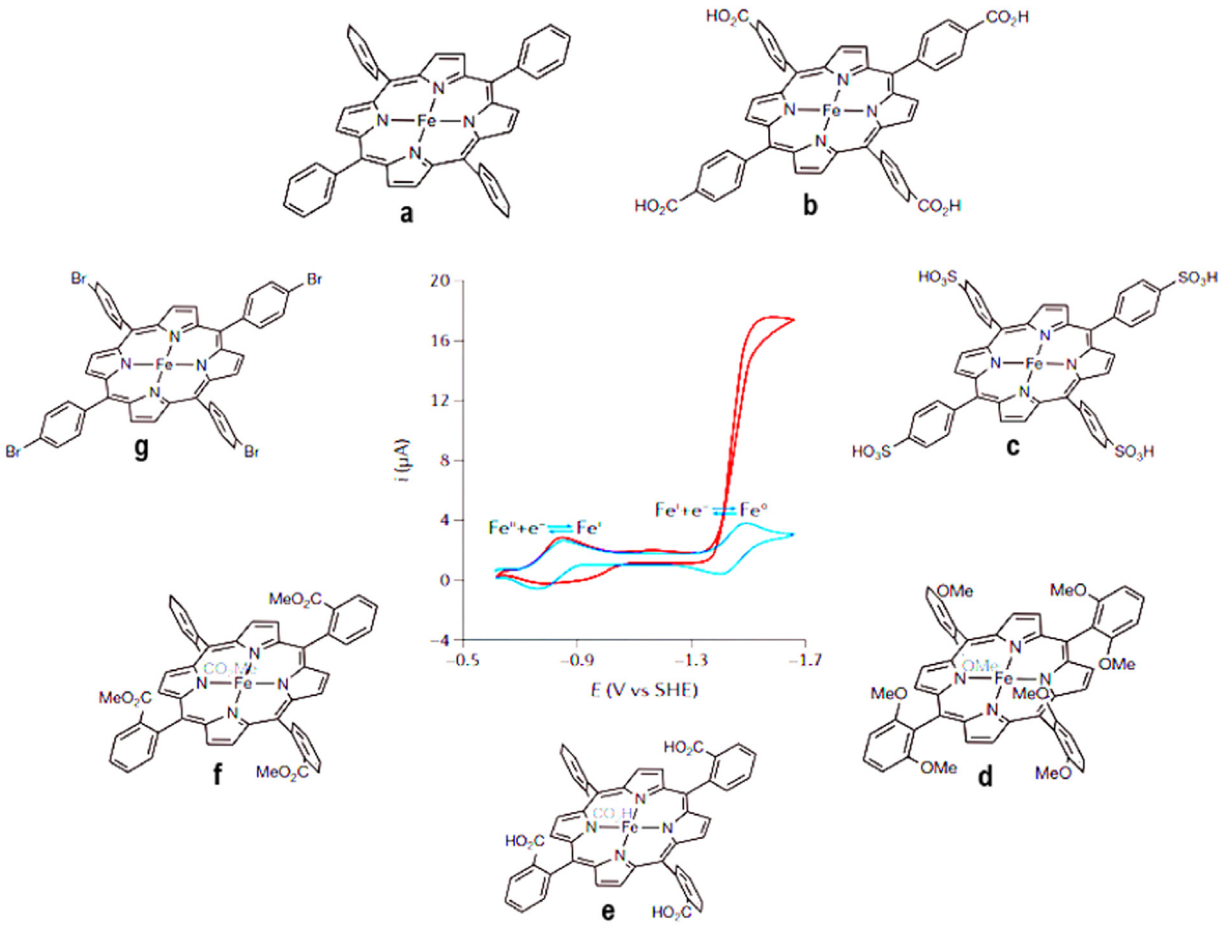

Fig. 4. Molecular structure of porphyrin derivatives and cyclic voltammograms of [Fe(TPP)] [51].

$TMPyFe^{3+}P$ catalyst, but with the other axial ligands, $TMPyFe^{3+}P$ proceeded to outer-sphere e-transfer ORR. On the other hand, to create a heterogeneous molecular catalyst, Cao et al. [68] adopted a similar strategy, attaching FePc to single-walled carbon nanotubes via linking pyridine at an axial position of FePc (Fig. 6(a)). The electrocatalytic ORR experiments demonstrated that the produced catalyst outperformed the standard Pt/C catalyst in terms of activity and durability (Fig. 6(b, c)). Theoretical studies showed that the ORR was significantly improved due to a dramatic shift in electronic as well as geometric structures of FePc brought about by the re-hybridization of 3d-orbitals of Fe with the axial pyridine orbitals.

In addition to the axial effect, the substituent position effect can also affect the catalytic activity of molecular electrocatalysts. As these molecular systems possess e- rich as well as e- poor substitution sites on their molecular core, therefore, EDG/EWG on such positions will affect the d-orbital of the central metal ion, altering the catalytic activity of the catalyst. For instance, Lv et al. [69] examined the effect of substituent position on the ORR activity of 2,4,6-OMe-CoP and 3,4,5-OMe-CoP (Fig. 6(d, e)) in a different study. According to the findings, 3,4,5-OMe-CoP showed effective ORR activity and good durability in comparison to 2,4,6-OMe-CoP (Fig. 6(f-i)). Due to the presence of the -OMe group on the reactive sites of CoP, 3,4,5-OMe-CoP exhibits increased charge as well as mass transfer, and hydrophilicity, endowing its ORR performance. This work presents an efficient approach for further enhancing catalytic activity by introducing the effect of substituent location on molecular electrocatalysts. These reports verify the effects of axial ligation as well as substituents position on the ORR performance of heterogeneous (molecular systems immobilized on carbon/material support) as well as homogeneous molecular catalysts and provide novel approaches for the rational design of low-cost, long-lasting intelligent molecular electrocatalysts for electrocatalytic ORR.

3.3. Through the M(III)/(II) redox potential

During oxygen reduction reaction (ORR), molecular catalysts' M(III)/(II) redox potential often acts as redox mediators, particularly those containing Mn and Fe transition metals. It is believed that maximum ORR activity may be reached if M(III)/(II) redox potential is close to O_2 reduction potential [70]. Therefore, M(III)/(II) Redox Potential can be considered the key activity descriptor for porphyry-type molecular catalysts of Mn and Fe transition metals. Since the M(III)/(II) redox potential of the molecular catalysts is associated with the eg-orbital of the central metal atom, the shifting of M(III)/(II) redox potential in the anodic region (up-shift in e_g energy level) brings about the fine-tuning of their ORR activity. This anodic shift in M(III)/(II) redox potential can be achieved via electron-withdrawing group substitution on their molecular framework (in the case of Fe and Mn-phthalocyanines, whereas it is vice versa for Co-porphyrins). Fig. 7(a) demonstrated the plots of ORR activities in basic media as current densities divided by the number of electrons involved in the reaction (n) for various metallophthalocyanines, supporting the crucial role of M(III)/(II) redox potential in ORR activity [53]. Within this framework, the theoretical aspects were also investigated by several research groups, and the results suggested that peripheral substitution on the molecular framework of metallo-porphyrins [11,71] as well as metallo-

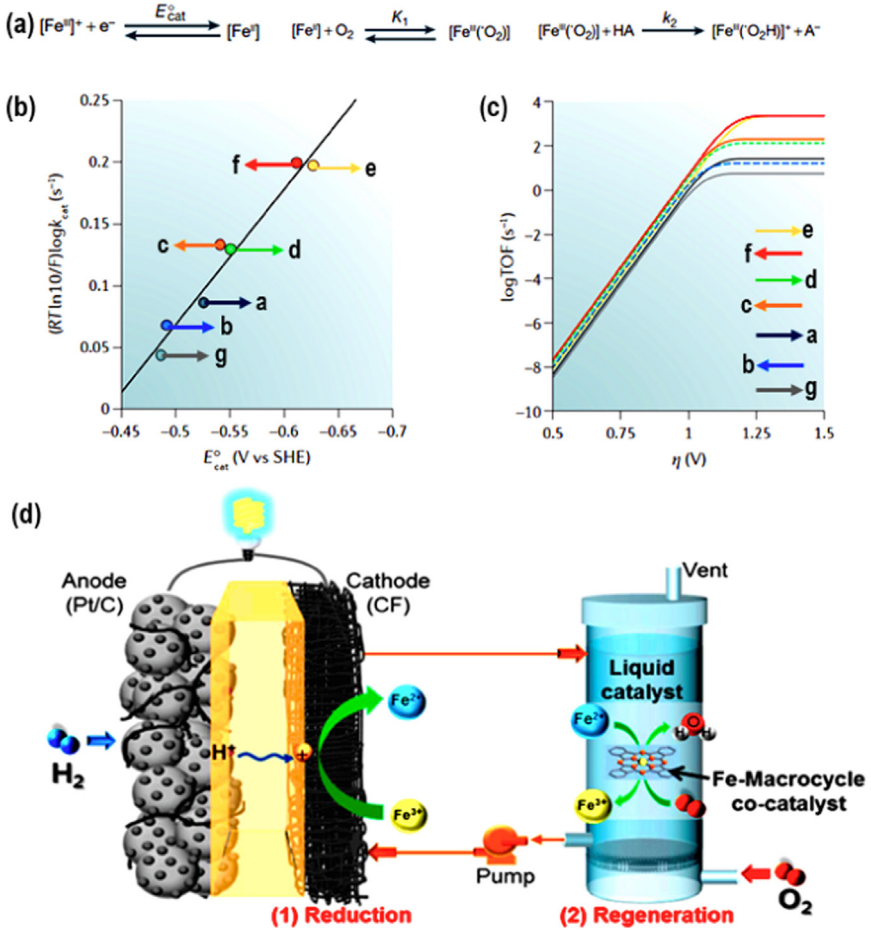

Fig. 5. (a) Role of Fe^{3+}/Fe^{2+} as mediator during ORR. (b) The Hammett-type linear correlation between logTOF (k_{cat}) and $E°_{cat}$ of Fe^{3+}/Fe^{2+} redox couple for FeP molecular catalysts. And the corresponding (c) Tafel plots shifting diagonally towards higher rates as well as higher overpotential with the EDGs. Taken with permission [51]. Copyrights 2017, American Chemical Society publishing group. (d) Representation of a chemically regenerative redox fuel cell using FePc as redox mediator catalyst. Adapted with permission [61], Copyright 2019 American Chemical Society publishing group.

phthalocyanines [72–75] could significantly alter their ORR activities, and the enhancement in their ORR activity was ascribed to the change in the energy of their d-orbital center. Therefore, molecular designers are putting their efforts into scripting the ideal molecular catalyst, having M(III)/(II) redox potential close to ORR potential to offer the best coupling between the ORR onset potential and M(III)/(II) redox potential, thereby achieving the highest ORR activity.

Abe et al. [76] adsorbed Fe-azaphthalocyanine (FeAzPc) on oxidized multiwall carbon nanotubes (ox-MWCNTs) in dimethyl sulfoxide (DMSO) and tested for ORR activity (Fig. 7(b)). The results exhibited superior ORR with far better durability compared to parent FePc and commercial Pt/C due to the electron-withdrawing (EW) properties of the pyridinic-N atoms in FeAzPcs. The EW nature of pyridinic-N atoms in FeAzPcs decreased the electron density of Fe-sites, resulting in an anodic shift in Fe(III)/(II) redox potential, which acted as an ORR mediator, as compared to FePc, thereby, enhancing the ORR activity of FeAzPc (Fig. 7(c)). Further, in order to support the FeN_4 moieties as the active sites for ORR in FeAzPc, they performed an ORR test in KCN and found that CN-ions were adsorbed on Fe-sites, reducing the overall ORR performance of the FeAzPc catalyst (Fig. 7(d)). This work opens the door to possibilities for designing similar analogues of FePc with strong EWGs on their molecular core to improve the ORR performance of porphyry-type molecular systems further.

Considering the similar concept of Fe(III)/(II) redox potential and enhancement of active site density in ORR, Zhang et al. [77] polymerized iron-phthalocyanine (pFePc) via a one-pot microwave-assisted strategy (Fig. 7(e)). The pFePc displayed extremely high ORR performance, showing activity much better than that of the FePc monomer and 20 wt% Pt/C. The increased ORR activity of pFePc over monomeric FePc was attributed to a shift in the Fe(III)/(II) redox potential in the anodic region caused by increased pi-pi conjugation (Fig. 7(f, g)). Moreover, an edge-closing protocol has been proposed with the aim of enhancing the stability of pFePc in a basic environment via the removal of edge anhydride groups. The best performance of high-power density as high as 452 mW/cm^2 is reported using edge-closed pFePc as a cathode catalyst in alkaline polymer electrolyte membrane fuel cells.

Recently, our research group also prepared conjugated poly-FePc through the polymerization of 1,2,4,5-tetracyanobenzene in the presence of $FeCl_2$ in microwave conditions. The prepared poly-FePc was tested for its ORR activity, and the results demonstrated that poly-FePc exhibited higher ORR activity than monomeric FePc, and the improved ORR activity of poly-FePc could be attributed to the extended pi-pi conjugation in poly-FePc, which could significantly shift the Fe(III)/(II) redox potential in the anodic region, which acted as an ORR mediator, enhancing the ORR activity of poly-FePc than monomeric FePc (Fig. 7(h, i)) [78]. Theoretical studies demonstrated that the $4e^-$ ORR pathway was followed because

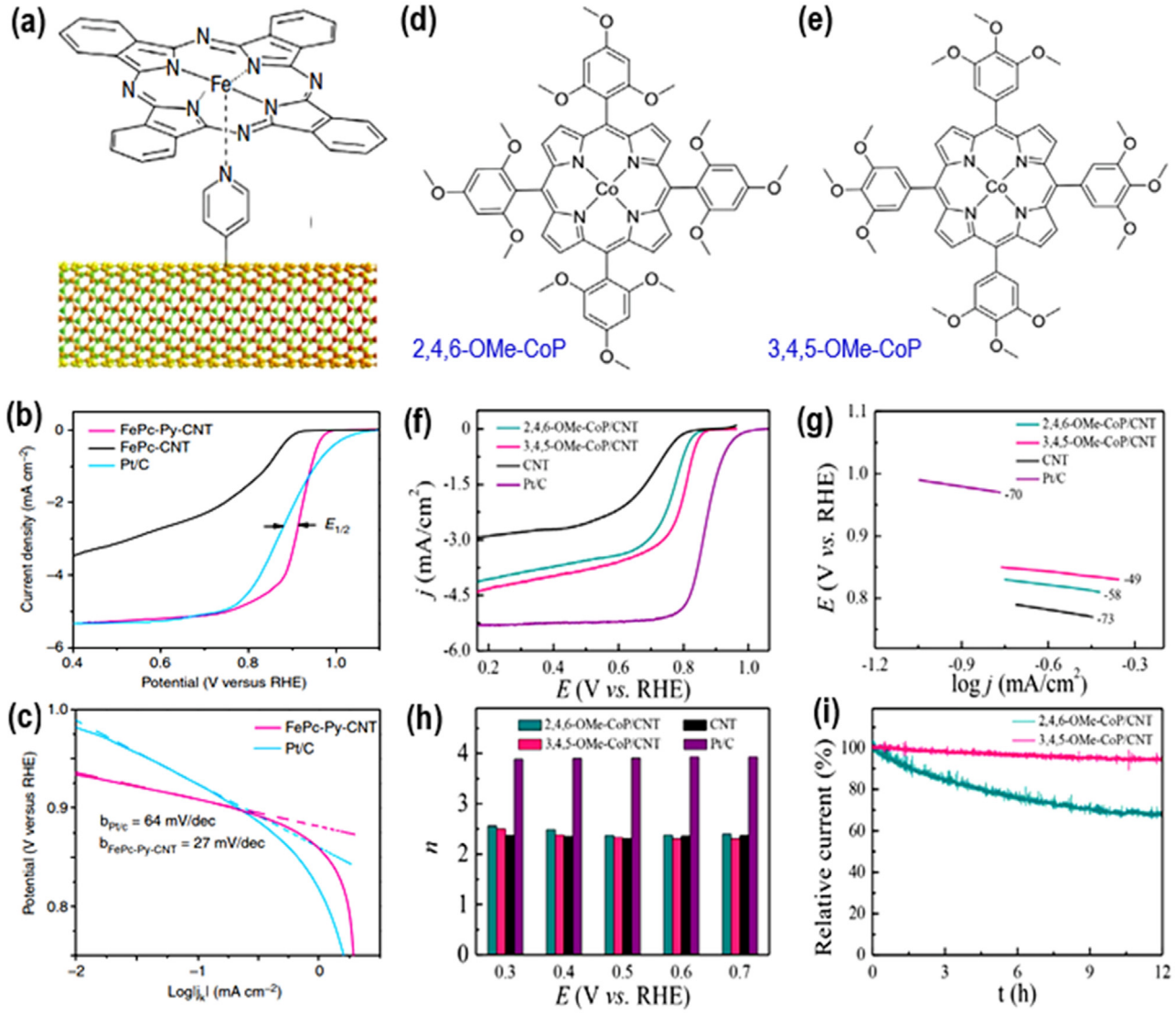

Fig. 6. (a) Systematic representation of CNTs-pyridine axially coordination with FePc. (b) ORR LSVs of FePc-CNTs, FePc-Py-CNTs, and Pt/C catalysts. (c) ORR Tafel plots for the FePc-Py-CNTs and Pt/C electrocatalysts. Taken with permission [68]. Copyrights 2013, Elsevier publishing group. Chemical structures of (d) 2,4,6-OMe-CoP and (e) 3,4,5-OMe-CoP, molecular catalysts. (f) LSV curves, (g) Tafel slopes, and (h) e^- transfer number of the molecular electrocatalysts during ORR. (i) The stability plot for both the 2,4,6-OMe-CoP and 3,4,5-OMe-CoP molecular electrocatalysts. Taken with permission [69]. Copyrights 2021, Nature publishing group.

the significant conjugation in poly-FePc lowered the energy of the dz^2-orbital of Fe, putting it closer to the pi*-orbital of O_2. The findings of this study revealed that modifying the electrical topologies of the molecular catalysts could improve ORR performance.

Further, Venegas et al. [79] reported the effect of fifth coordination on the Fe(III)/(II) redox couple and, as a result, on the ORR activity of the $_{16}$(Cl)FePc molecular catalyst in a similar manner. Fig. 8(a) illustrates the CNTs modified with pyridine (CNTs-Py) in N_2 saturated 0.1 M H_2SO_4 electrolyte and FeN_4 (FePc as well as $_{16}$(Cl)FePc) in the presence or absence of a Py-axial link. The results show that the Fe(III)/(II) redox couple has a higher redox potential in $_{16}$(Cl)FePc than in unsaturated FePc, which may be due to the distribution of the electron-withdrawing Cl-group across the Ph-ligand. The basic nature of CNTs makes them capable of changing the electron density of Fe via pi-pi electronic communication. ORR catalysis is favoured by the shift of Fe(III)/(II) redox potential to the anodic region (Fig. 8(b, c)) [4,30]. Fig. 1(c) represents H_2O_2 production corroborated by a rotating ring disc electrode (RRDE). The formation of H_2O_2 becomes more pronounced if the axial ligand is absent. CNTs-$_{16}$(Cl)FePc is the most potent catalyst for H_2O_2 production, while Py ligand is reported to reduce H_2O_2 production to very low levels (Fig. 8(d)). The reason may be the decoupling of the metal center due to coordination from CNTs, which eventually helps alter the geometrical and electronic structure to restrict the H_2O_2 formation. Further, they suggested that although the activity of $_{16}$(Cl)FePc was not higher compared to FePc, the EWGs (Cl) on FePc disfavour the coupling of O_2 with Fe, resulting in a mismatch in the energy of the frontier orbitals, which shifted the Fe(III)/(II) redox potential (Fig. 8(e)) and thus lowered the ORR activity.

3.4. Through controlling the M-O_2 binding energy

It is established that metal (M)-O_2 binding energy ($E_{b(O2)}$) on molecular catalysts can be controlled via chemical modification of the molecular core of the catalysts. For instance, the volcanic relationship between ($E_b(O_2)$) and ORR activity demonstrated that Fe-based molecular catalysts with high O_2-affinity enhanced ORR activity, while Co-based molecular catalysts displayed lower ORR activity since they had a poor affinity for O_2, as shown in Fig. 9(a) [53]. This idea was also correlated with the M(III)/(II) redox po-

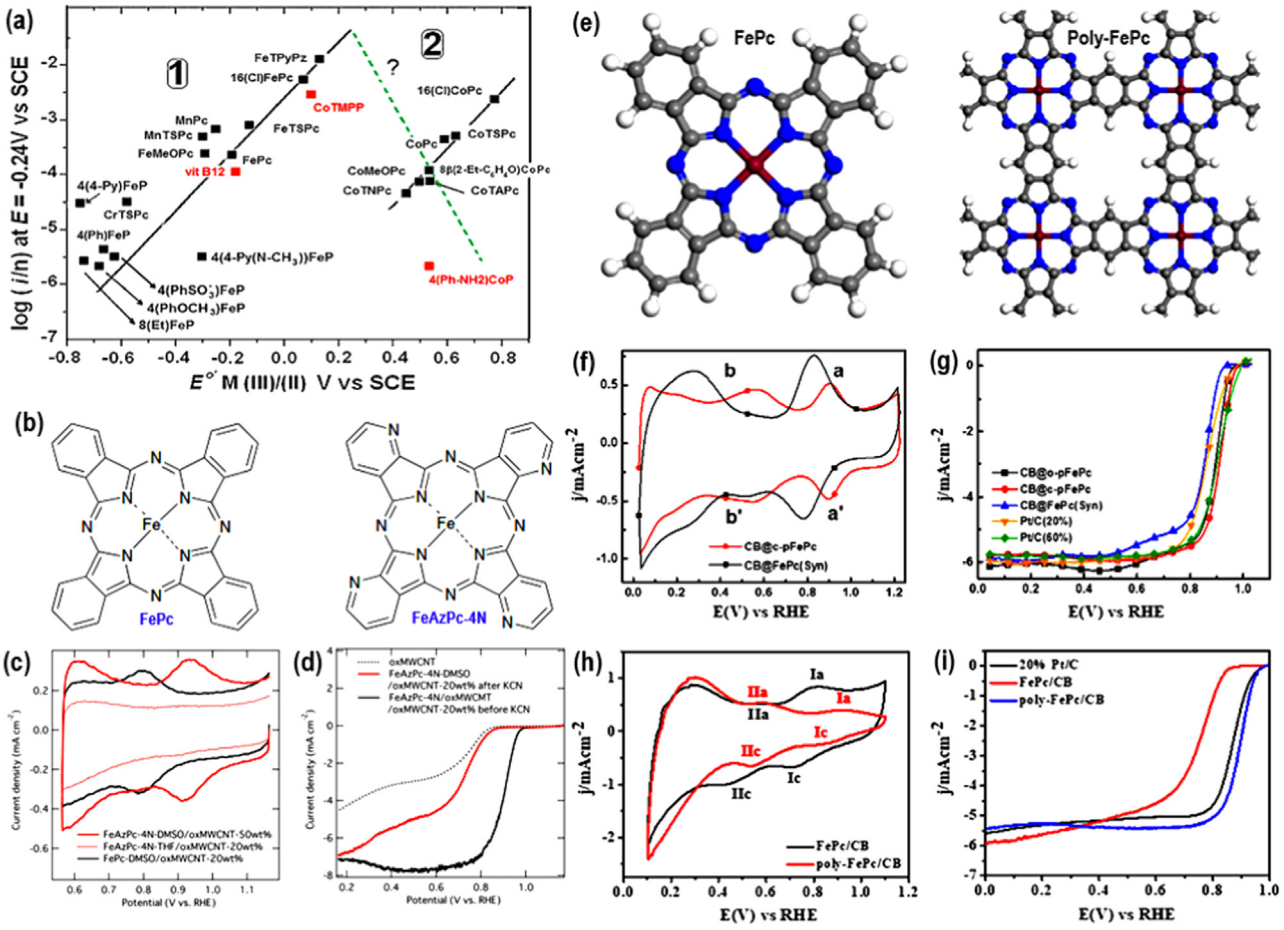

Fig. 7. (a) Plots between ORR activities and current densities for various molecular electrocatalysts in an alkaline environment. Adopted with permission [53], copyrights, 2019. Elsevier publishing group. (b) Chemistry structure of FePc and iron-tetra-2,3-pyridinoporphyrazine (FeAzPc-4N). (c) CV curves for FePc, and FeAzPc-4N composites in N_2-saturated 0.1 M KOH. (d) LSVs for FePc, and FeAzPc-4N composites in O_2-saturated 0.1 M KOH before (black) and after (red) the addition of 10 mM KCN [76]. (e) Chemistry structure, (f) CVs, and (g) LSVs, of monomeric FePc and poly-FePc (p-FePc). Adopted with permission [77], copyrights, 2019. ACS publishing group. (h) CVs recorded in N_2-saturated 0.1 M KOH, and (i) LSVs, of monomeric FePc, poly-FePc, and 20% Pt/C. Adopted with permission [78], copyrights, 2022. Elsevier publishing group.

tential, suggesting that EWGs on the molecular core are capable of shifting the M(III)/(II) redox potential (for Fe and Mn-based catalysts, in particular) in the anodic region. In contrast, for Co-based molecular catalysts, the M(II)/(I) redox couple acts as an ORR mediator; therefore, the EDGs enhance their O_2 binding affinity and thus help in improving the ORR activity. Within this approach, Sun et al. [80] used the density of functional theory (DFT) calculation on Fe- and Co-based molecular catalysts to figure out the link between (Eb(O_2)) and ORR activity. Fig. 9(b) displays the optimum energy levels for the M-O_2 adducts in the B3 states of FePc and CoPc. On the basis of the data, it seems that the Pcs framework includes both occupied (1u) and unoccupied ($2e_g$) molecular orbitals, as well as a1g (dz^2), b1g (dx^2-y^2), 1e_g (d_{zx}, d_{yz}), and b_{2g} (d_{xy}) 3d-orbitals, and the eg-orbitals of FePc, being more energetic than CoPc, can contribute electron density into the pi*-orbital of O_2 easily to weaken the O-O bond and thus endow high ORR activity (Fig. 9(b)).

Apart from the above, there is also a correlation between a molecular catalyst's ionization potential (IP) and its O_2-binding capacity, as proposed by Shi et al. [81]. Ionic potential (IP) and charge over the catalyst molecules are the two most crucial factors in determining O_2-binding capacity. It was hypothesized that ORR activity would improve in proportion to increases in IP and O_2-binding energy. According to DFT investigations, different types of central metal ions, ligands, and EW/ED-substituents affect the molecular catalyst's O_2-binding ability. The EDGs increase and EWGs decrease the O_2-binding capacity of CoPcs (Fig. 9(c)). It is possible to account for the observed ORR activity pattern in phthalocyanines and porphyrin frameworks by considering their IP and O_2-binding capabilities.

On the other hand, Hui et al. [82] used DFT simulations to confirm the electronic effect of O_2, OH, and H_2O_2 species on the Fe/Co-based molecular catalysts. The putative adsorption energy of ORR intermediates (OH and H_2O_2) and O_2 molecules adsorbed on different Fe- and Co-based molecular catalysts is shown in Fig. 9(d). Typically, the adsorption energy of ORR intermediates (OH* and H_2O_2*) was proportional to the adsorption energy of O_2 on the catalyst (O_2*). On the basis of their theoretical results, they suggested that (i) adsorption energies of O_2 and ORR intermediates (OH and H_2O_2) on the molecular catalysts are mostly determined by the type of metal center, (ii) adsorption of O_2 and ORR intermediates on molecular catalysts can be modified through EDG/EWG substitution on the molecular framework, and (iii) in order to support the effective 4e$^-$ ORR route, it is necessary to disrupt the O-O link, which necessitates N-M-N like structures with an appropriate N-to-N distance and N-to-M electronic collaboration [159].

3.5. Through inductive electronic effects

A positive influence on either the overpotential or the TOF may result from the substituents having an inductive electronic impact on the framework of the molecular catalyst. This con-

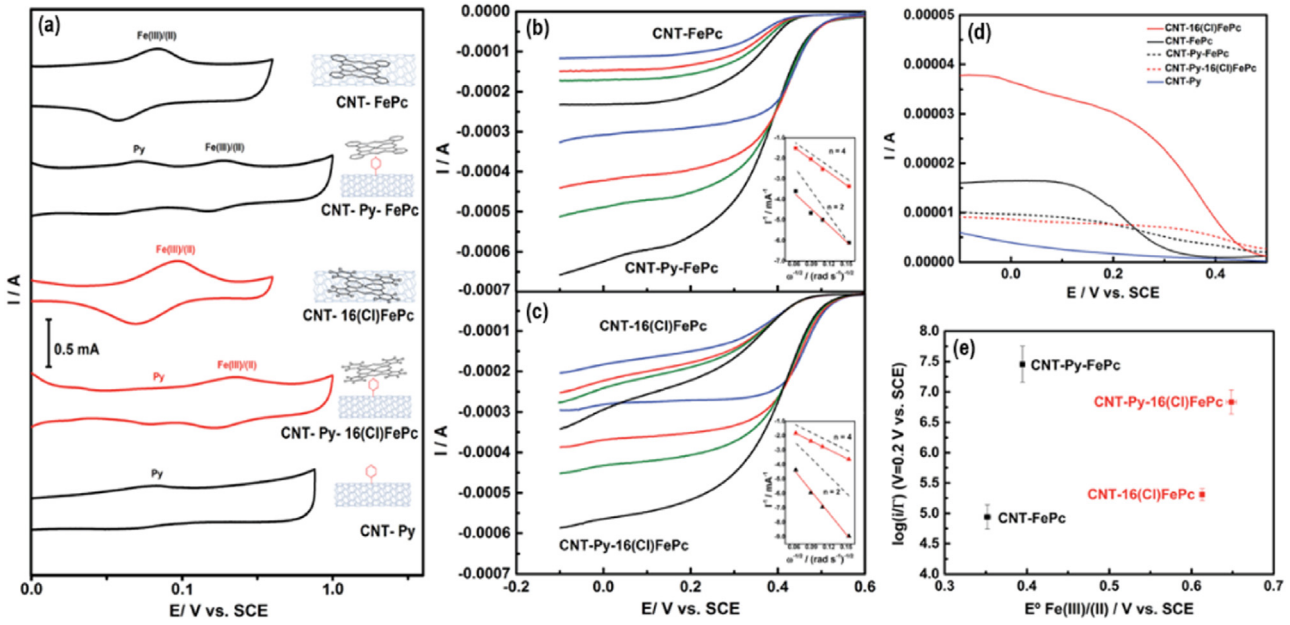

Fig. 8. (a) CVs, and (b) LSVs, of CNT-FePc, CNT-Py-FePc, CNT-16(Cl) FePc, CNT-Py-$_{16}$(Cl)FePc, and CNT-Py, recorded in N_2 and O_2-saturated 0.1 M H_2SO_4 solution at 100 mV/s and 5 mV/s scan rate, respectively. (b) H_2O_2 oxidation activity on Pt ring electrode; (c) ORR polarization curves for CNT-16(Cl) FePc and CNT-Py-$_{16}$(Cl)FePc recorded in O_2-saturated 0.1 M H_2SO_4 solution at 5 mV/s scan rate. (d) H_2O_2 produced at Pt ring electrode with CNT-16(Cl)FePc; or CNT-FePc; CNT-Py-FePc; CNT-Py-16(Cl)FePc; or CNT-Py in O_2-saturated 0.1 M H_2SO_4 solution. (e) Plots between ORR activity (log *i*/*G*) and Fe(III)/(II) redox potential, recorded in O_2 saturated 0.1 M H_2SO_4. Adopted with permission [79], copyrights, 2022. Royal Society of Chemistry Publishing group.

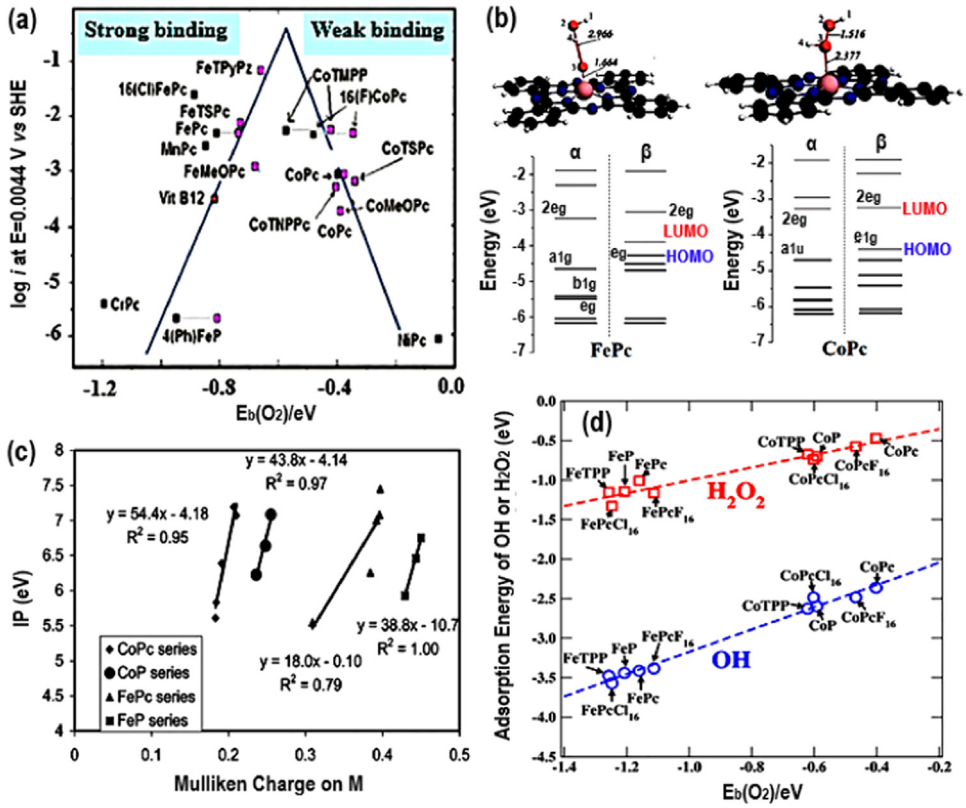

Fig. 9. (a) Volcano relationships between ORR activity and O_2 binding energy on various metallo-phthalocyanines. Adopted with permission [53]. Copyrights 2017, American Chemical Society Publishing Group. Elsevier publishing group. (b) Optimized M-O_2 adducts at the B3 state for (a) FePc, (b) CoPc, with corresponding Energy levels (a = spin-down orbital; b = spin-up orbital), Adopted with permission [80]. Copyrights 2019, American chemical society publishing group. (c) Correlations between Mulliken charges on central metal and IPs for various metallo-phthalocyanines. Adopted with permission [81]. Copyrights 2007, American Chemical Society Publishing Group. (d) Relationships between calculated adsorption energy of the OH (blue circles)/H_2O_2 (red squares) and calculated adsorption energy of the O_2 on the Fe and Co-based molecular catalysts. Reproduced with permission [82]. Copyright 2019, American Chemical Society Publishing Group.

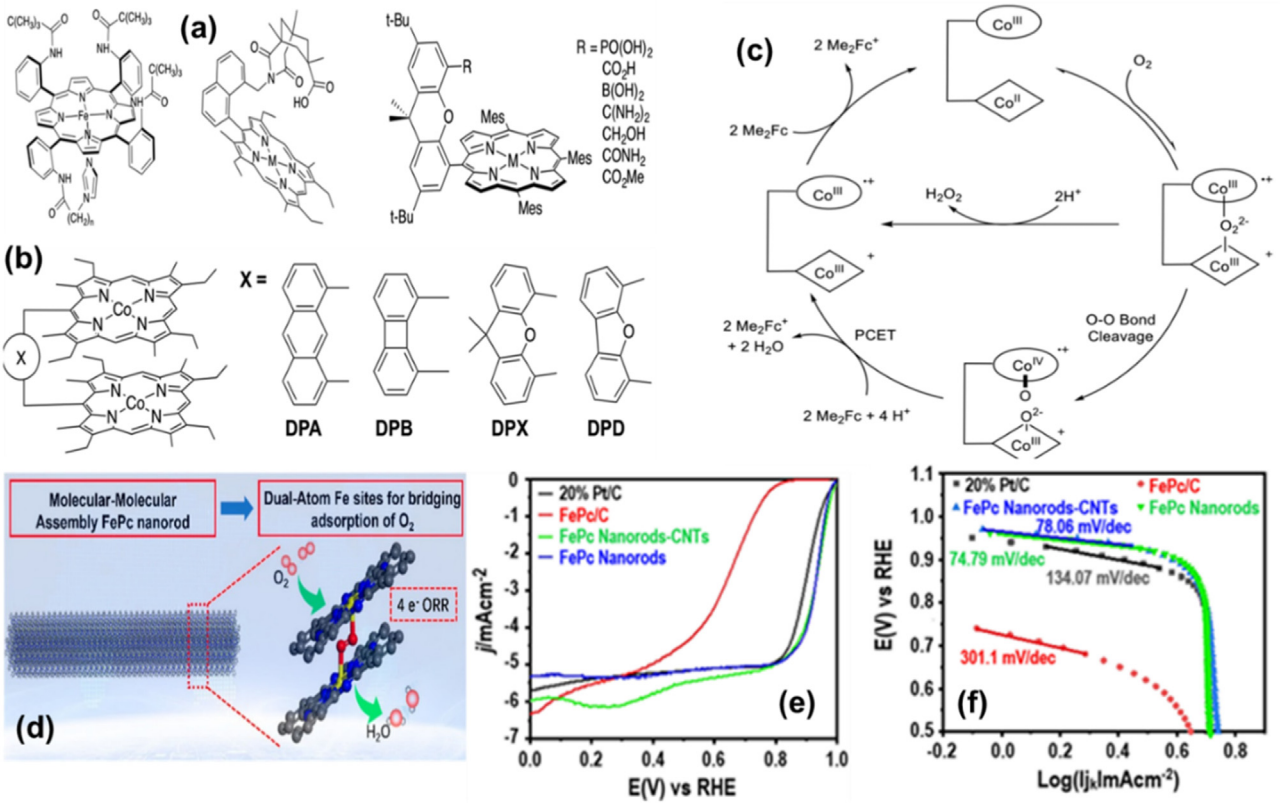

Fig. 10. Chemical structures for the (a) Collman, Chang, and Hangman's porphyrin-based molecular models [86]. (b) Cofacial Co-porphyrin-based molecular electrocatalysts for ORR catalysts. Taken with permission [90]. Copyrights 2009, American Chemical Society Publishing Group. (c) The expected ORR mechanism with the selectivity-determining step [90]. (d) Graphical abstract of co-facial arrangement of FePcs in 1D architecture, (e) LSV curves, and (f) Tafel plots of the monomeric FePc, co-facial FePc, and Pt/C catalysts. Taken with permission [91]. Copyrights 2022, American Chemical Society Publishing Group.

cept may allow for more realistic experimental circumstances, even if such molecular electrocatalysts can only lead to diagonal moves in catalytic Tafel plots. However, overcoming the limitations as per the 'Iron rule' by components affecting the catalyst's electronic structure under the influence of inductive effect is a much more formidable challenge. The key intermediates can be stabilized by both through-structure effects and the spatially extended functions of some substituents [83]. These effects could be caused by the electrostatic attraction or repulsion that occurs between charged substituents. The ORR serves as a classic illustration of this principle, in this case, the tetra(2-pyridyl) FeP manages to avoid the linearity of the 'iron law' relationship [84]. This is explained by the fact that 2-pyridyl substituents can undergo protonation to offer electrostatic action. Through-space effects in molecular catalysts, like environmental effects that occur at active sites contained by enzymes with non-anticipated influential effects [85].

3.6. Through the secondary coordination-sphere effects

Many attempts have been made to boost the ORR performance of molecular electrocatalysts by imitating the effects of consolidating and stimulating the O_2-adducts of metalloenzymes [86]. These attempts have been met with varying the secondary coordination sphere (SCS) in molecular electrocatalysts, modifying the electronic structure of active sites and their ability towards O_2 binding as well as O_2 activation [87–89]. These SCS effects originate from the hydrogen-bonding donors (HBDs) and Lewis acid moieties in the molecular framework of the catalyst during the ORR process.

One of the key challenges in the early stages of O_2-binding investigations was to examine the differences in the relative binding strengths of O_2 and CO with the Fe-site of the porphyrin ring in haemoglobin and myoglobin, which strongly favors CO [92,93]. It has been determined through many studies [94,95] that the presence of HBDs in the active site pocket is responsible for this difference. It is hypothesized that the HBDs have the capability of stabilizing the bound superoxide adduct. In addition, a wide range of porphyrin-based molecular catalysts that have HBDs in the SCS has been designed, synthesized, and evaluated for their potential to facilitate the electrocatalytic ORR. The formation of unfavorable dimers and oxo-adducts by metallo-porphyrins can be prevented by HBDs, as these factors limit the ORR activity of molecular electrocatalysts. The HBDs not only raise the affinity for O_2 binding, but also raise ORR activity. For instance, several research groups [93,96,97] have constructed molecular catalysts with acidic groups or HBDs serving as H^+ relays and investigated the electrocatalytic ORR [98–101] (Fig. 10(a)). The O-O link rupture can be promoted directly by the presence of acidic groups or HBDs near the O_2-binding site [102,103], which is a crucial fundamental step in regulating ORR activity with high selectivity.

3.7. Through the co-facial dual atom sites

In traditional molecular catalyst research, covalently coupled co-facial dual-atomic molecular electrocatalysts for ORR have drawn a lot of attention in addition to monomeric molecular catalysts. The majority of single-atomic molecular catalysts exhibit $2e^-$ ORR, generating H_2O_2. This has prompted the scientific community to develop co-facial molecular structures to stabilize the per-

Table 1
ORR performance of some porphyry-type molecular electrocatalysts.

Molecular electrocatalysts	Electrolyte	E_{Onset} (V)	$E_{1/2}$ (V)	Refs.
Face-to-face stacked nanorods	0.1 M KOH	+0.97 V *vs* RHE	+0.91 V *vs* RHE	[91]
Face-to-face stacked iron phthalocyanine	0.1 M KOH	-0.04 *vs* SCE	-0.14 *vs* SCE	[91]
Face-to-face stacked cobalt phthalocyanine	0.1 M KOH	-0.20 *vs* SCE	-0.34 *vs* SCE	[106]
Face-to-face stacked zinc phthalocyanine	0.1 M KOH	-0.30 *vs* SCE	-0.43 *vs* SCE	[106]
Iron phthalocyanine/Graphene oxide	0.1 M KOH	-	-0.32 *vs* SCE	[74]
Iron phthalocyanine/ Graphene oxide/ Multi-walled carbon nanotubes	0.1 M KOH	-0.07 *vs* SCE	-	[74]
Tetra-CP substituted iron phthalocyanine	0.1 M KOH	-0.069 *vs* SCE	-0.23 *vs* SCE	[107]
Iron phthalocyanine/Carbon black	0.1 M H_2SO_4	-0.09 *vs* $Hg/HgSO_4$	-	[108]
Bi-nuclear iron phthalocyanine/Carbon black	0.1 M H_2SO_4	-0.01 *vs* $Hg/HgSO_4$	-	[108]
Iron phthalocyanine/N-doped graphene sheets	0.1 M H_2SO_4	-0.02 *vs* $Hg/HgSO_4$	-	[108]
Bi-nuclear iron phthalocyanine/N-doped graphene sheets	0.1 M H_2SO_4	0.12 *vs* $Hg/HgSO_4$	-	[108]
Iron porphyrin/graphene	0.1 M KOH	+0.98 V *vs* RHE	+0.88 V *vs* RHE	[109]
Cobalt porphyrin/Reduced graphene oxide	0.5 M KOH	+0.98 V *vs* RHE	+0.88 V *vs* RHE	[110]
Iron porphyrin/Reduced graphene oxide	0.1 M KOH	+0.95 V *vs* RHE	+0.86 V *vs* RHE	[111]
Iron porphyrin/Multi-walled carbon nanotubes	0.1 M $HClO_4$	+1.0 V *vs* RHE	+0.88 V *vs* RHE	[112]
Hemin/CNTs/Reduced graphene oxide	0.1 M KOH	+0.98 V *vs* RHE	+0.89 V *vs* RHE	[113]
Hemin/Carbon nanotubes	0.1 M KOH	+0.91 V *vs* RHE	+0.81 V *vs* RHE	[113]
Hemin/Reduced graphene oxide	0.1 M KOH	+0.94 V *vs* RHE	+0.86 V *vs* RHE	[113]
Hemin/Carbon black	0.1 M KOH	+0.92 V *vs* RHE	+0.78 V *vs* RHE	[114]
Heat-treated hemin/ Carbon black	0.1 M KOH	+1.0 V *vs* RHE	+0.86 V *vs* RHE	[114]

oxide intermediate and prefer $4H^+/4e^-$ ORR, via direct O-O linkage breaking [91,104]. Although most co-facial molecular systems have been immobilized on carbon electrode surfaces as heterogeneous electrocatalysts and tested for ORR performance, recent studies have shown that they also have excellent ORR activity in a homogeneous phase, and their catalytic properties are highly dependent on the distance and angle between both active sites incorporated into the co-facial molecular framework [86,90,105]. Co-facial porphyrins (Fig. 10(b)), for example, showed ORR in PhCN with $HClO_4$ and Me_2Fc. Due to the formation of a Co-O-O-Co adduct between both Co-active sites, only these molecular catalysts possess $4e^-$ ORR with high selectivity [105]. The kinetic investigation of this catalyst revealed that RDS is dependent on the reductant concentration, so the reaction was classified as a first-order reaction. Furthermore, the experimental rate laws suggested that proton-coupled electron transfer (PCET) from Co^{3+}/Co^{2+} to O_2 with the Me_2Fc immediately began the intramolecular O-O bond breakage with the $Me_{10}Fc$, resulting in a $4e^-$ mechanism during ORR (Fig. 10(c)).

Besides the significant development, single or dual-atomic molecular electrocatalysts still do not possess satisfactory durability during ORR. It can be attributed to the de-metalation of the metal active site in the electrolyte from their molecular framework, losing their performance, and it is therefore very challenging to realize molecular catalysts for practical use in energy devices. Hence, there is a need to develop several strategies to benchmark the performance of such molecular electrocatalysts, enabling the replacement of costly materials in such technologies [51]. The most important aspect of molecular electrocatalysts is their transformation from molecular phase to stable and redox-active 1D/2D/3D engineering (using covalent, non-covalent, or coordination-based strategies) to make them usable at a practical level with superior performance in energy conversion devices. Very recently, our research group constructed 1D architecture (nanorods) incorporating the FePc molecules in co-facial arrangement (Fig. 10(d)) [91]. The constructed FePc architecture displayed excellent ORR performance in terms of activity, selectively as well as durability (Fig. 10(e, f)). The findings of advanced characterization techniques suggested that O_2 was inserted between two Fe-sites, forming a trans Fe-O-O-Fe adduct, which facilitated the fast ORR (direct O-O bonding rupture), avoiding H_2O_2 formation. Table 1 shows the ORR performance of some porphyry-type molecular electrocatalysts.

4. Conclusions

4.1. Summary

To sum up, the search for suitable alternatives to expensive Pt electrocatalysts for ORR is still going on for the advancement of fuel cell technology. Among various developed classes of electrocatalysts, porphyry-type molecular catalysts have been used as promising ORR catalysts. This article discusses the thermodynamics of ORR for a fundamental understanding of the ORR mechanism with molecular electrocatalysts. Further, it deals with the fundamental chemistry of molecular catalysts, highlighting their electronic and electrochemical features and correlations with electrocatalytic ORR activity, and discussing the volcano plots under the guidance of Sabatier's principle.

Depending on the nature of the active site and type of molecular core, these molecular models offer end-on or side-on adsorption configurations for O_2 on the central single-atom site, displaying $4e^-/2e^-$ ORR process. Under the light of activity descriptors, including redox potential, O_2-binding energy, frontier energy levels (HOMO-LUMO), the close proximity of dual-atom sites, ionization potential, and Mullikan charge on the central metal atom, the ORR activity and selectivity of porphyry-based molecular catalysts can be controlled by modifying them chemically. On the other hand, understanding volcano plots for 'O_2 binding energy vs. activity' and 'redox potential vs. activity' provides a useful prospect for the tailoring of porphyry catalysts to improve their catalytic ORR activity.

According to the findings of these volcano plots, electron-withdrawing group-substituted Fe-based molecular electrocatalysts display an anodic shift in Fe(III)/Fe(II) redox potential, improving the O_2 binding energy on the Fe-site, thereby enhancing the ORR catalytic activity. Since the M(III)/M(II) redox potential represents the eg-orbital of molecular electrocatalysts, the optimum electronic coupling between the eg-orbital of molecular systems and π^*-orbital of O_2 will represent the onset potential of the ORR polarization curve. This fact opens the door for the further modification of molecular electrocatalysts to achieve their desirable ORR performance.

Also, porphyry-type molecular models with co-facial arrangements can provide the precise configuration of dual-atomic sites for the mutual coordination of both the O-atoms of O_2, forming a

cis- or trans-O_2 adduct and, as a result, a direct breaking of the O-O bond, which makes them more selective for $4e^-$ ORR.This strategy can be extended to the design of various dual-atomic molecular as well as metal-nitrogen-carbon materials. Although ongoing advancements have been achieved for porphyry-type molecular electrocatalysts for ORR, several issues with these catalysts related to the precise control of the electronic structure of the central active site, limited activity, and durability remain to be addressed, as discussed in the next subsection.

4.2. Challenges and future prospects

Applying the Sabatier rule and analyzing the volcano plots of current vs. thermodynamic parameters is an appealing strategy for optimizing molecular electrocatalysts, offering many advantages to characterize catalytic reactions, and create novel electrocatalysts with benchmark performance. This fascination is not simply due to the breathtaking landscapes that it inspires, but also because electrocatalysis is described via a single variable. Both of these factors contribute to the overall appeal of this approach. Nevertheless, it is believed that a catalytic reaction cannot be conceived as a solitary elementary process, and this strategy is not relevant to a large number of molecular catalysts. This is because a catalytic reaction involves more than one elementary step. On the other hand, the primary intermediate's free energy is not the only criterion for describing catalytic processes. This is why it seems that standard catalysts are more fruitful than volcano hunting. In addition, the catalytic Tafel plots, which establish a relationship between TOF and overpotential, make it possible to provide a more comprehensive explanation of the kinetics of catalysis. It also serves as a solid foundation for standard catalysts and evaluating novel concepts in catalyst design. The catalytic Tafel plot associates many parameters that regulate the catalytic activity of the catalysts, and therefore, more precise investigations on these concepts are required to invent the ideal molecular catalyst for ORR.

On the other hand, a thorough and extensive study for incorporating suitable components into the catalyst structure to have an inductive effect on the active site is required to interplay via space instead of the catalyst's framework to get around the so-called "iron rule". The electrochemical conversion of dioxygen to water by substituted porphyry-type molecular systems has been improved via space effects under the influence of electrostatic as well as hydrogen bonding, nevertheless, advanced research is required to apply these concepts to molecular catalysis. In this context, quantum chemical calculations may have a potential role in chemical ingenuity. However, it is crucial to remember that comparative estimations that demonstrate a tendency are dependable compared to actual values, especially those that are derived from the most cutting-edge methods. Therefore, a physico-mathematical investigation is required in order to find the bare minimum number of non-dimensional regulating parameters. This is a preferred approach for utilizing 'theoretical simulation' methodologies, however, it does require one to assess all experimental resources, such as scan rate effect and change, order of reaction of the catalyst, substrate, and co-substrate. Repetition of tests/methods is necessary if a new catalyst needs to be produced to derive mechanistic knowledge.

Moreover, although substantial efforts are made for the durability enhancement of porphyry-type molecular electrocatalysts, these electrocatalysts still exhibit poor stability. To remedy this problem, it may be necessary to investigate the concept of thermal-treatment and conductive materials as support in order to identify the most likely solution to enhance their stability during catalytic operation. Fig. 11 illustrates the linking of (i) molecular models and their catalytic activity, controlling the activity descriptors, (ii) activity and durability, employing the concepts of material science, and (iii) durability and molecular models, measuring the electrocatalytic parameters to approach the molecular catalysts at large scale. In addition, precursors used in the fabrication of molecular catalysts are expensive. In addition, the procedures involved in the creation of molecular catalysts are costly, rendering the entire endeavor unfeasible from an economic point of view. Discovering inexpensive precursors is necessary for resolving these difficulties. Extensive research is required to find a low-cost method for producing molecular catalysts, reducing the total cost to a level where these electrocatalysts can be used commercially. This schematic representation of molecular catalysts with other components from fundamental chemistry, material science, and electrochemistry shows the possibilities and future directions for designing efficient molecular catalysts for ORR. We hope this review article will assist readers in gaining a better understanding of fundamental scientific and engineering concepts to design effective molecular and atomically dispersed single-atom/dual-atom metal-nitrogen-carbon (M-N-C) electrocatalysts and to comprehend their ORR mechanism, over potential, TOF, catalytic Tafel plots, etc.

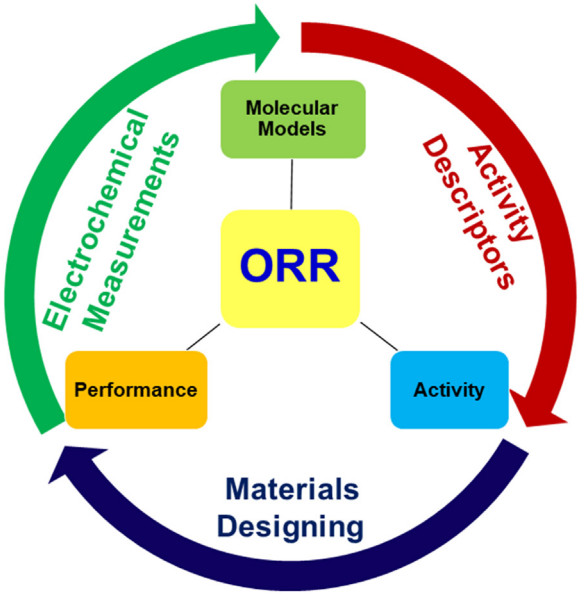

Fig. 11. Schematic representation of molecular catalysts with other components from fundamental chemistry, material science, and electrochemistry to design efficient molecular catalysts for ORR.

Declaration of Competing Interest

The authors declare that they have no known competing financial interests or personal relationships that could have appeared to influence the work reported in this paper.

Acknowledgment

The authors extend their appreciation to the Deanship of Scientific Research at King Khalid University for funding this work through large group Research Project under grant number RGP2/172/44.

References

[1] F. Razi, I. Dincer, Renew. Sust. Energ. Rev. 168 (2022) 112763.
[2] J. Yang, D.W. Kang, H. Kim, B. Hwang, J.W. Lee, Chem. Eng. J. 451 (2023) 138909.

[3] Z. Li, A. Kumar, N. Liu, M. Cheng, C. Zhao, X. Meng, H. Li, Y. Zhang, Z. Liu, G. Zhang, J. Mater. Chem. A 10 (2022) 14355–14363.
[4] G. Yasin, S. Ibrahim, S. Ajmal, S. Ibraheem, S. Ali, A.K. Nadda, G. Zhang, J. Kaur, T. Maiyalagan, R.K. Gupta, Coord. Chem. Rev. 469 (2022) 214669.
[5] S.D. Bhoyate, J. Kim, F.M. de Souza, J. Lin, E. Lee, A. Kumar, R.K. Gupta, Coord. Chem. Rev. 474 (2023) 214854.
[6] Y. Wang, X. Zheng, D. Wang, Nano Res. 15 (2022) 1730–1752.
[7] G. Zhang, X. Li, K. Chen, Y. Guo, D. Ma, K. Chu, Angew. Chem.-Int. Edit. 62 (2023) e202300054.
[8] H.J. Chen, R. Wang, Y.L. Yang, X.L. Shi, S. Lu, Z.G. Chen, Prog. Nat. Sci. 31 (2021) 858–864.
[9] G. Zhou, G. Liu, X. Liu, Q. Yu, H. Mao, Z. Xiao, L. Wang, Adv. Funct. Mater. 32 (2022) 2107608.
[10] R. Jasinski, J. Electrochem. Soc. 112 (1965) 526.
[11] J. Van Veen, J. Van Baar, C. Kroese, J. Coolegem, N. De Wit, H. Colijn, Ber. Bunsenges. Phys. Chem. 85 (1981) 693–700.
[12] J.H. Zagal, M.A. Páez, J. Silva, in: N4-Macrocyclic Metal Complexes, Springer Verlag, 2006, pp. 41–82.
[13] A. Kumar, G. Zhang, W. Liu, X. Sun, J. Electroanal. Chem. 922 (2022) 116799.
[14] A. Kumar, G. Yasin, S. Ajmal, S. Ali, M.A. Mushtaq, M.M. Makhlouf, T.A. Nguyen, P. Bocchetta, R.K. Gupta, S. Ibraheem, Int. J. Hydrog. Energy 47 (2022) 17621–17629.
[15] J.R. van Veen, C. Visser, Electrochim. Acta 24 (1979) 921–928.
[16] Y. Wang, Z. Zhang, X. Zhang, Y. Yuan, Z. Jiang, H. Zheng, Y.G. Wang, H. Zhou, Y. Liang, CCS Chem. 4 (2022) 228–236.
[17] X. Luo, R. Abazari, M. Tahir, W.K. Fan, A. Kumar, T. Kalhorizadeh, A.M. Kirillov, A.R. Amani-Ghadim, J. Chen, Y. Zhou, Coord. Chem. Rev. 461 (2022) 214505.
[18] A. Kumar, S. Ibraheem, T.A. Nguyen, R.K. Gupta, T. Maiyalagan, G. Yasin, Coord. Chem. Rev. 446 (2021) 214122.
[19] R. Li, D. Wang, Nano Res. 15 (2022) 6888–6923.
[20] A. Kumar, V.K. Vashistha, D.K. Das, Coord. Chem. Rev. 431 (2021) 213678.
[21] C. Costentin, J.M. Savéant, Nat. Rev. Chem. 1 (2017) 1–8.
[22] S. Bhunia, A. Ghatak, A. Dey, Chem. Rev. 122 (2022) 12370–12426.
[23] E. Cook, C. Machan, Chem. Commun. 84 (2022) 11746–11761.
[24] I. Soni, P. Kumar, G.K. Jayaprakash, Coord. Chem. Rev. 472 (2022) 214782.
[25] X. Wang, L. Guo, Z. Xie, X. Peng, X. Yu, X. Yang, Z. Lu, X. Zhang, L. Li, Appl. Surf. Sci. 606 (2022) 154749.
[26] J.S. Bates, M.R. Johnson, F. Khamespanah, T.W. Root, S.S. Stahl, Chem. Rev. 123 (2022) 6233–6256.
[27] C. Costentin, H. Dridi, J.M. Savéant, J. Am. Chem. Soc. 137 (2015) 13535–13544.
[28] C. Costentin, J.M. Savéant, ChemElectroChem 1 (2014) 1226–1236.
[29] C. Costentin, J.M. Savéant, J. Am. Chem. Soc. 140 (2018) 16669–16675.
[30] P.M. Osterberg, J.K. Niemeier, C.J. Welch, J.M. Hawkins, J.R. Martinelli, T.E. Johnson, T.W. Root, S.S. Stahl, Org. Process. Res. Dev. 19 (2015) 1537–1543.
[31] D.J. Wasylenko, C. Rodríguez, M.L. Pegis, J.M. Mayer, J. Am. Chem. Soc. 136 (2014) 12544–12547.
[32] M.L. Pegis, C.F. Wise, D.J. Martin, J.M. Mayer, Chem. Rev. 118 (2018) 2340–2391.
[33] J.J. Warren, T.A. Tronic, J.M. Mayer, Chem. Rev. 110 (2010) 6961–7001.
[34] C. Costentin, S. Drouet, M. Robert, J.-M. Savéant, J. Am. Chem. Soc. 134 (2012) 11235–11242.
[35] V. Artero, J.-M. Saveant, Energy Environ. Sci. 7 (2014) 3808–3814.
[36] J.A. Roberts, R.M. Bullock, Inorg. Chem. 52 (2013) 3823–3835.
[37] M.L. Pegis, J.A. Roberts, D.J. Wasylenko, E.A. Mader, A.M. Appel, J.M. Mayer, Inorg. Chem. 54 (2015) 11883–11888.
[38] Q. Liu, R. Liu, C. He, C. Xia, W. Guo, Z.L. Xu, B.Y. Xia, eScience 2 (2022) 453–466.
[39] M.L. Pegis, B.A. McKeown, N. Kumar, K. Lang, D.J. Wasylenko, X.P. Zhang, S. Raugei, J.M. Mayer, ACS Cent. Sci. 2 (2016) 850–856.
[40] M.L. Helm, M.P. Stewart, R.M. Bullock, M.R. DuBois, D.L. DuBois, Science 333 (2011) 863–866.
[41] W.A. Hoffert, J.A. Roberts, R.M. Bullock, M.L. Helm, Chem. Commun. 49 (2013) 7767–7769.
[42] C.T. Carver, B.D. Matson, J.M. Mayer, J. Am. Chem. Soc. 134 (2012) 5444–5447.
[43] W.R. Barros, T. Ereno, A.C. Tavares, M.R. Lanza, ChemElectroChem 2 (2015) 714–719.
[44] M.L. Pegis, C.F. Wise, B. Koronkiewicz, J.M. Mayer, J. Am. Chem. Soc. 139 (2017) 11000–11003.
[45] F. Shi, L. Zhai, Q. Liu, J. Yu, S.P. Lau, B.Y. Xia, Z.L. Xu, J. Energy Chem. 76 (2023) 127–145.
[46] M. Che, Catal. Today 218 (2013) 162–171.
[47] M. Koper, J. Solid State Electrochem. 17 (2013) 339–344.
[48] P. Quaino, F. Juarez, E. Santos, W. Schmickler, Beilstein J. Nanotechnol. 5 (2014) 846–854.
[49] A.R. Zeradjanin, J.P. Grote, G. Polymeros, K.J. Mayrhofer, Electroanalysis 28 (2016) 2256–2269.
[50] J.M. Savéant, Chem. Rev. 108 (2008) 2348–2378.
[51] C. Costentin, J.M. Savéant, J. Am. Chem. Soc. 139 (2017) 8245–8250.
[52] C. Costentin, J.M. Savéant, ACS Appl. Mater. Interfaces 9 (2017) 19894–19899.
[53] J.H. Zagal, M.T. Koper, Angew. Chem.-Int. Edit. 55 (2016) 14510–14521.
[54] J.H. Zagal, S. Specchia, P. Atanassov, Curr. Opin. Electrochem. 27 (2021) 100683.
[55] S. Specchia, P. Atanassov, J.H. Zagal, Curr. Opin. Electrochem. 27 (2021) 100687.
[56] A. Kumar, Y. Zhang, Y. Jia, W. Liu, X. Sun, Chinese J. Catal. 42 (2021) 1404–1412.
[57] J.H. Zagal, M. Gulppi, M. Isaacs, G. Cárdenas-Jirón, M.J. ś Aguirre, Electrochim. Acta 44 (1998) 1349–1357.
[58] J. Ouyang, K. Shigehara, A. Yamada, F.C. Anson, J. Electroanal. Chem. Interfacial Electrochem. 297 (1991) 489–498.
[59] C. Shi, F.C. Anson, Inorg. Chem. 29 (1990) 4298–4305.
[60] H. Niu, C. Xia, L. Huang, S. Zaman, T. Maiyalagan, W. Guo, B. You, B.Y. Xia, Chin. J. Catal. 43 (2022) 1459–1472.
[61] S.B. Han, D.H. Kwak, H.S. Park, I.A. Choi, J.Y. Park, K.B. Ma, J.E. Won, D.H. Kim, S.J. Kim, M.C. Kim, ACS Catal. 6 (2016) 5302–5306.
[62] J.H. Dawson, Science 240 (1988) 433–439.
[63] I.M. Rietjens, A.M. Osman, C. Veeger, O. Zakharieva, J. Antony, M. Grodzicki, A.X. Trautwein, J. Biol. Inorg. Chem. 1 (1996) 372–376.
[64] T.L. Poulos, J. Biol. Inorg. Chem. 1 (1996) 356–359.
[65] D.B. Goodin, J. Biol. Inorg. Chem. 1 (1996) 360–363.
[66] R.A. Matute, A. Toro-Labbé, M.P. Oyarzún, S. Ramirez, D.E. Ortega, K. Oyarce, N. Silva, J.H. Zagal, Electrochim. Acta 391 (2021) 138905.
[67] D. Solomon, P. Peretz, M. Faraggi, J. Phys. Chem. C 86 (1982) 1842–1849.
[68] R. Cao, R. Thapa, H. Kim, X. Xu, M. Gyu Kim, Q. Li, N. Park, M. Liu, J. Cho, Nat. Commun. 4 (2013) 1–7.
[69] H. Lv, H. Guo, K. Guo, H. Lei, W. Zhang, H. Zheng, Z. Liang, R. Cao, Chin. Chem. Lett. 32 (2021) 2841–2845.
[70] A. van der Putten, A. Elzing, W. Visscher, E. Barendrecht, J. Electroanal. Chem. Interfacial Electrochem. 221 (1987) 95–104.
[71] E. Theodoridou, A. Jannakoudakis, P. Jannakoudakis, S. Antoniadou, J. Besenhard, J. Appl. Electrochem. 22 (1992) 733–737.
[72] J.P. Randin, Electrochim. Acta 19 (1974) 83–85.
[73] F. Beck, J. Appl. Electrochem. 7 (1977) 239–245.
[74] J.H. Zagal, Coord. Chem. Rev. 119 (1992) 89–136.
[75] J. Zagal, M. Paez, A. Tanaka, J. dos Santos Jr, C. Linkous, J. Electroanal. Chem. 339 (1992) 13–30.
[76] H. Abe, Y. Hirai, S. Ikeda, Y. Matsuo, H. Matsuyama, J. Nakamura, T. Matsue, H. Yabu, NPG Asia Mater. 11 (2019) 1–12.
[77] H. Zhang, S. Zhang, Y. Wang, J. Si, Y. Chen, L. Zhuang, S. Chen, ACS Appl. Mater. Interfaces 10 (2018) 28664–28671.
[78] A. Kumar, G. Yasin, M. Tabish, D.K. Das, S. Ajmal, A.K. Nadda, G. Zhang, T. Maiyalagan, A. Saad, R.K. Gupta, J. Chem. Eng. 445 (2022) 136784.
[79] R. Venegas, F.J. Recio, J. Riquelme, K. Neira, J.F. Marco, I. Ponce, J.H. Zagal, F. Tasca, J. Mater. Chem. A 5 (2017) 12054–12059.
[80] S. Sun, N. Jiang, D. Xia, J. Phys. Chem. C 115 (2011) 9511–9517.
[81] Z. Shi, J. Zhang, J. Phys. Chem. C 111 (2007) 7084–7090.
[82] H. He, Y. Lei, C. Xiao, D. Chu, R. Chen, G. Wang, J. Phys. Chem. C 116 (2012) 16038–16046.
[83] C. Renault, C.P. Andrieux, R.T. Tucker, M.J. Brett, V.R. Balland, B. Limoges, J. Am. Chem. Soc. 134 (2012) 6834–6845.
[84] M.P. Frushicheva, M.J. Mills, P. Schopf, M.K. Singh, R.B. Prasad, A. Warshel, Curr. Opin. Chem. Biol. 21 (2014) 56–62.
[85] J.P. Klinman, Acc. Chem. Res. 40 (2007) 325–333.
[86] S. Fukuzumi, K. Okamoto, Y. Tokuda, C.P. Gros, R. Guilard, J. Am. Chem. Soc. 126 (2004) 17059–17066.
[87] L.M. Mirica, X. Ottenwaelder, T.D.P. Stack, Chem. Rev. 104 (2004) 1013–1046.
[88] E.A. Lewis, W.B. Tolman, Chem. Rev. 104 (2004) 1047–1076.
[89] A. Borovik, Acc. Chem. Res. 38 (2004) 54–61.
[90] K.M. Kadish, L. Frémond, J. Shen, P. Chen, K. Ohkubo, S. Fukuzumi, M. El Ojaimi, C.P. Gros, J.-M. Barbe, R. Guilard, Inorg. Chem. 48 (2009) 2571–2582.
[91] A. Kumar, K. Sun, X. Duan, S. Tian, X. Sun, Chem. Mater. 34 (2022) 5598–5606.
[92] J.P. Collman, R. Boulatov, C.J. Sunderland, L. Fu, Chem. Rev. 104 (2004) 561–588.
[93] J.P. Collman, Acc. Chem. Res. 10 (1977) 265–272.
[94] T.G. Spiro, M.Z. Zgierski, P.M. Kozlowski, Coord. Chem. Rev. 219 (2001) 923–936.
[95] E. Sigfridsson, U. Ryde, J. Biol. Inorg. Chem. 4 (1999) 99–110.
[96] C.Y. Yeh, C.J. Chang, D.G. Nocera, J. Am. Chem. Soc. 123 (2001) 1513–1514.
[97] C. Chang, Y. Liang, G. Aviles, S.M. Peng, J. Am. Chem. Soc. 117 (1995) 4191–4192.
[98] J.D. Soper, S.V. Kryatov, E.V. Rybak-Akimova, D.G. Nocera, J. Am. Chem. Soc. 129 (2007) 5069–5075.
[99] D.K. Dogutan, S.A. Stoian, R. McGuire Jr, M. Schwalbe, T.S. Teets, D.G. Nocera, J. Am. Chem. Soc. 133 (2011) 131–140.
[100] J. Rosenthal, D.G. Nocera, Acc. Chem. Res. 40 (2007) 543–553.
[101] W. Zhang, W. Lai, R. Cao, Chem. Rev. 117 (2017) 3717–3797.
[102] L.L. Chng, C.J. Chang, D.G. Nocera, Org. Lett. 5 (2003) 2421–2424.
[103] B. Zyska, M. Schwalbe, Chem. Commun. 49 (2013) 3799–3801.
[104] J.P. Collman, P.S. Wagenknecht, J.E. Hutchison, Angew. Chem.-Int. Edit. 33 (1994) 1537–1554.
[105] S. Fukuzumi, K. Okamoto, C.P. Gros, R. Guilard, J. Am. Chem. Soc. 126 (2004) 10441–10449.
[106] N. Koçyiğit, Ü.E. Özen, M. Özer, B. Salih, A.R. Özkaya, Ö. Bekaroğlu, Electrochim. Acta 233 (2017) 237–248.
[107] J.P. Collman, C.S. Bencosme, C.E. Barnes, B.D. Miller, J. Am. Chem. Soc. 105 (1983) 2704–2710.
[108] N. Kobayashi, Y. Nishiyama, J. Phys. Chem. C 89 (1985) 1167–1170.
[109] H. Jahnke, M. Schönborn, G. Zimmermann, Top Curr. Chem. 61 (1976) 133–181.

[110] M. Jahan, Q.L. Bao, K.P. Loh, J. Am. Chem. Soc. 134 (2012) 6707–6713.
[111] S.K. Kim, S. Jeon, Electrochem. Commun. 22 (2012) 141–144.
[112] Y. He, G.Q. Yu, Y. Naruta, J.G. Liu, Angew. Chem.-Int. Edit. 53 (2014) 6659–6663.
[113] A. Kumar, G. Yasin, V.K. Vashistha, D.K. Das, M.U. Rehman, R. Iqbal, Z. Mo, T.A. Nguyen, Y. Slimani, M.T. Nazir, W. Zhao, Diam. Relat. Mater. 113 (2021) 108272.
[114] P.B. Xi, Z.X. Liang, S.J. Liao, Int. J. Hydrog. Energy 37 (2012) 4606–4611.